공학박사 학위논문

Manipulation of nanocracks on silicon based thin film and its application as large area nanopatterning

실리콘 기반의 박막을 이용한 나노 크렉의 제어 및 대면적 나노 패턴 제작으로서의 응용 기술에 대한 연구

2016 년 2 월

서울대학교 대학원

기계항공공학부 기계공학전공

Suh Young Duk

Manipulation of nanocracks on silicon based thin film and its application as large area nanopatterning

지도 교수 고 승 환

이 논문을 공학박사 학위논문으로 제출함
2016 년 2 월

서울대학교 대학원
기계항공공학부 기계공학전공
Suh Young Duk

Suh Young Duk의 공학박사 학위논문을 인준함
2015 년 12 월

위 원 장 전 누 리 (인)

부위원장 고 승 환 (인)

위 원 김 도 년 (인)

위 원 전 호 정 (인)

위 원 이 대 호 (인)

초 록

Generally, a fracture is considered as an uncontrollable phenomenon due to its highly random nature. The aim of this study is to investigate straight, random, and highly ordered cracks such as oscillatory cracks and to manipulate via elaborate control of mechanical properties of the cracking medium including thickness, geometry, and elastic mismatch. Utilizing semiconductor fabrication and laser technology, a specific thin film with micro-sized notches fabricated on a silicon based substrate generates various types of self-propagating nano-cracks in large area including optical wave-like nano-cracks resembling refraction, total internal reflection and evanescent wave. These novel properties are utilized to fabricate complex and large areal nano/micro patterns which is extremely difficult to fabricate using conventional nano/micro patterning process. The nano/micro patterns made in this study are directly implementable into a nano/micro-channel application since the cracks naturally have a form of channel-like shape. In addition, a flexible transparent conductor fabrication using the nano/micro patterns as template is demonstrated.

주요어 : Nanopatterning, fracture, crack, transparent conductor, crack assisted patterning
학 번 : 201430860

Table of Contents

Chapter 1.

Introduction

1.1. Background

Over the last several decades, nanopatterning techniques have been rapidly advanced along with semi-conductor technology. Nowadays, the demand for nanopatterning techniques are even greater and much more specific as various types of nanopatterns are required as a basis of different multi-disciplinary studies including nano-fluidics[1], nano-electronics[2] and nanoelectromechanical systems (NEMS)[3].

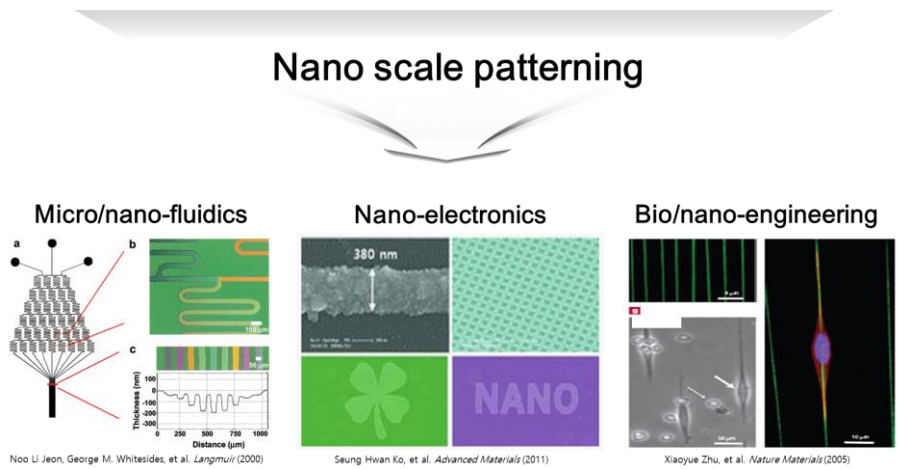

Figure 1. Various applicable areas of nanopatterning technology.

In these days, various nanopatterning techniques utilizing lithography as well as non-lithographic approaches are available.[4] As shown in Figure 2,

several techniques including electron beam lithography (EBL)[5], scanning probe microscopy (SPM)[6] or scanning tunneling microscopy (STM)[7], and atomic force microscopy (AFM)[8] guarantees nanoscale precision. The resolution of these techniques are highly precise, however the fabrication processes are often time consuming and expensive. In addition, serial processes are required for large area patterning since the maximum size of single process area of these techniques is usually smaller than 1cm x 1cm.

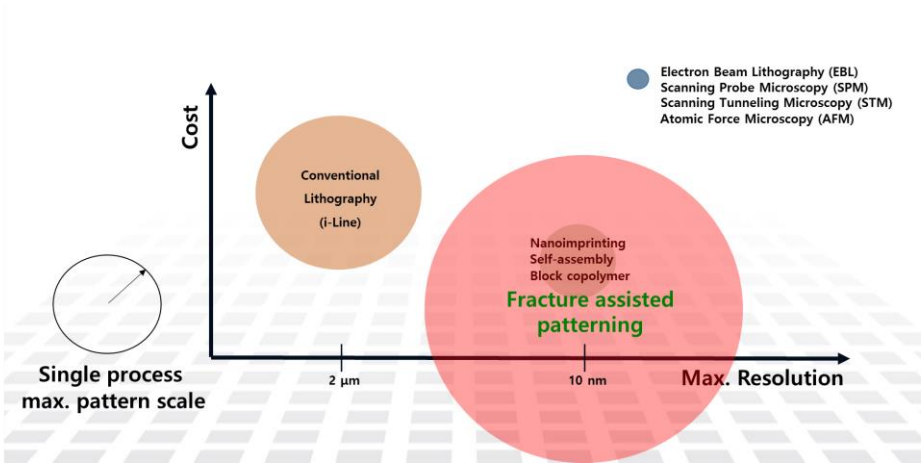

Figure 2. Various nanopatterning techniques. X and Y axis shows maximum resolution and cost respectively. Radius of each circle represents single process maximum pattern scale. Notice fracture assisted patterning has a potential for large area patterning.

On the other hand, nanoimprinting[9], self-assembly[10], and block-copolymer lithography[11] techniques have attained patterning capabilities equivalent or even better than conventional photo lithography at relatively lower cost.[12-15] These techniques are typically carried out under non-vacuum

and room temperature environment which leads to lesser equipment and cost reduction. Nevertheless, there are limitations of these techniques: resultant patterns are simple repetitive types, and fabrication of a master template which often involves the aid of state of art optical lithography technology. Foremost, both techniques are hindered by the difficulties of defect free fabrication over large area. For these reasons, large area nanopatterning is a challenging assignment.

1.1 Previous studies

Since discovery of cracking control in glass material by Yuse and Sano,[16] various research have introduced possibility of the cracking as a pattern former[17,18] especially in nano-fluidics[18,19]. In turn, awareness of using cracking as a viable candidate for nanopatterning technique have steadily emerged from being a totally random phenomenon[20,21].

Recently, the prospect of nanocrack as a pattern former has been revitalized by Koo et al.[22] Using chemical vapor deposition (CVD) of glassy material on a silicon substrate, precise control of initiation and stop of different propagation modes of fracture such as straight and oscillatory crack have been successfully demonstrated. The cracks in Koo's report showed great nanoscale features including extremely good line edge roughness (LER), line width roughness (LWR), and aspect ratio of width to depth.

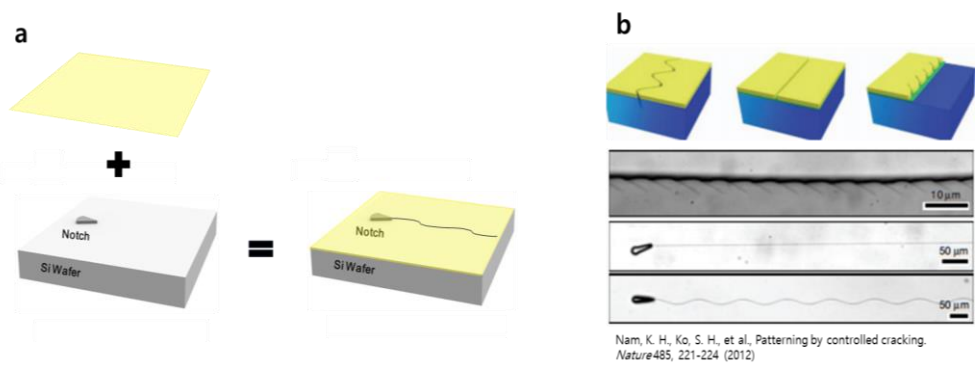

Figure 3. Controlled thin film fracture using semiconductor process. (a) Schematic process showing generation of controlled fracture of glassy thin film deposited using semiconductor process. (b) Tailored nanocracks having

different propagation modes demonstrate precise control. Notice high aspect ratio of the crack i.e. length vs. width.

Another similar attempt has been made by Donghyun Kim et al.[23] by utilizing differential thermal expansion of glassy films on a metal patterned silicon substrate. Although there have been some instabilities in the oscillation of the crack, control of wave parameters of the oscillatory crack has been successfully demonstrated in micro scale. Both studies showed a remarkable control of naturally propagating oscillatory cracks as a mean of nanopatterning.

The crack control demonstrated in these studies is, however, limited in several aspects. First of all, the crack patterns are simple as in straight or oscillatory form. In order to create a complicated or complex pattern, the notch structures which initiate the crack must be predefined. This requires an additional patterning process. In addition, novel properties of the oscillatory cracks such as amplitude and wavelength have not been studied deeply although these properties have significant potential for higher complexity patterns if controlled properly. Another limitation is the pattern width which is typically in 100 nm regime. This extremely fine scale pattern width limits the use unless another state of art nanotechnology which provides equivalent resolution is involved. Since most of the state of art technologies have limited process area, the significance of using cracks as large area patterning appears to be less impactful. For these reasons, there

have been no direct applications using the concept of patterning by nanocracking.

1.2. Objective

In an attempt to expand this prospective phenomenon even further for various applications including nano/micro channel fabrication and transparent conductor panel fabrication, elaborate control of the various cracks including initiation, stop, and manipulation at a specific location or within a region of interest while maintaining high aspect ratio and low LER, LWR using CVD deposition of glassy thin films on a silicon as well as theoretical background is studied. The oscillatory cracks fabricated in this manor exhibit optical wave-like properties such as refraction, total internal reflection and evanescent wave. Utilizing these properties enable various nanopatterns which are directly applicable to nanochannel fabrication. In addition, randomly occurring cracks provide a good utility especially when used as a template for transparent conductor fabrication via selective etching and pattern widening. The fabrication process of the transparent conductor and its applications are also demonstrated in this study.

Chapter 2.

Generation and manipulation of nanocracks

2.1. Thin film cracking by residual stress of Si_3N_4 on silicon substrate

The thin films used in this study are glassy materials such as Silicon Nitride (Si_3N_4) and Silicon dioxide (SiO_2) deposited by chemical vapor deposition (CVD) and by thermal oxidation of silicon wafer, respectively. These thin films generate high residual stress in the film and the substrate deposited upon especially when deposited at high temperature. The silicon nitride film deposited through low pressure chemical vapor deposition (LPCVD) process induces high tensile stress, approximately 1.0 dynes/cm^2·10^{10} (~1·GPa) in the film at room temperature.[24] Typically, thicker than 400 nm Si_3N_4 film deposition on the silicon substrate is avoided since the chance of film cracking is greatly increased at this stress and film thickness regime. In this study, the cracks are generated using this typically avoided process: high tensile stress induced by LPCVD silicon nitride (Si_3N_4) deposition process. As shown in Figure 4a, b, and c, the cracks occurred on the silicon substrate have different propagation characteristics which we believe mainly depend on the thickness of thin film and strain energy stored in the thin

film/substrate system. As the film thickness is increased extensively, large scale randomness of the cracking is reduced and repeatable random patterns appear as shown in Figure 4d. Details of this mechanism are discussed in the later chapters.

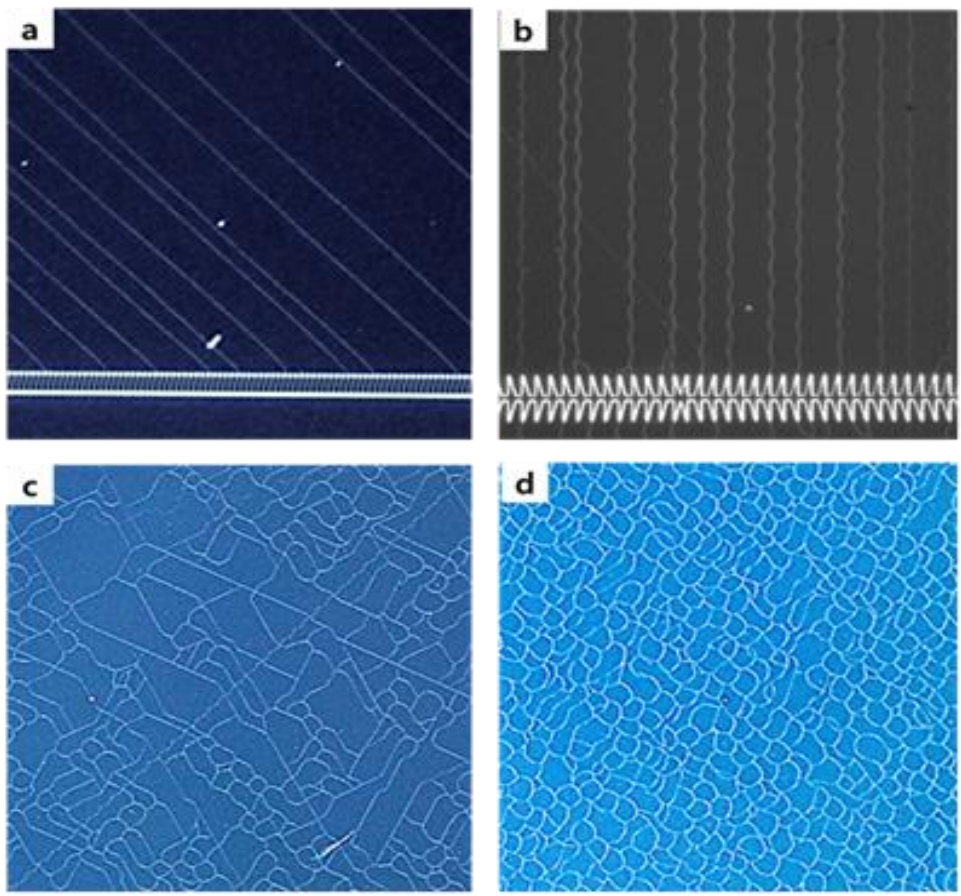

Figure 4. Various crack propagation modes: (a) Straight mode (b) Oscillatory mode (c) Randomly mixed mode (d) Fish scale-like catastrophic fracture.

Typical crack generation and control process used in this study is illustrated in Figure 5. Silicon substrates with three different

crystallographic orientations, (100), (110), and (111) are cleaned by standard wafer cleaning procedure: Piranha cleaning followed by HF (1:10, HF: H_2O) dip for native oxide removal. For crack initiation, notch-like structures are patterned on the substrates via photolithography followed by reactive ion etching (RIE). Subsequently, a 200 nm-thick silicon dioxide (SiO_2) thin film layer is grown on the patterned substrate by thermal oxidation (at 900˚C, 3 hrs.). The final SiO_2 patterns are defined by photolithographic patterning followed by RIE. In order to control the thickness of SiO_2 patterns, the substrates are wet etched in diluted HF solution (1:20). Various silicon dioxide film patterns are employed to study the propagation characteristics of a crack. As a final step, a stoichiometric silicon nitride (Si_3N_4) film was deposited on the substrates by chemical vapor deposition (CVD). The temperature and pressure condition of CVD were 800 ℃ and 200 mtorr, respectively. In order to induce high residual stress in the silicon nitride film, dichlorosilane (H_2SiCl_2) and ammonia (NH_3) at 30 cm^3 min^{-1} (STP) and 100 cm^3 min^{-1} (STP) were used respectively. The cracks self-propagate on the substrates during or after the CVD process. When the substrates are taken out from the CVD chamber, the final crack patterns are already defined, thus no additional process is required. The substrates were then characterized and analyzed by scanning electron microscopy (SEM) and optical microscope.

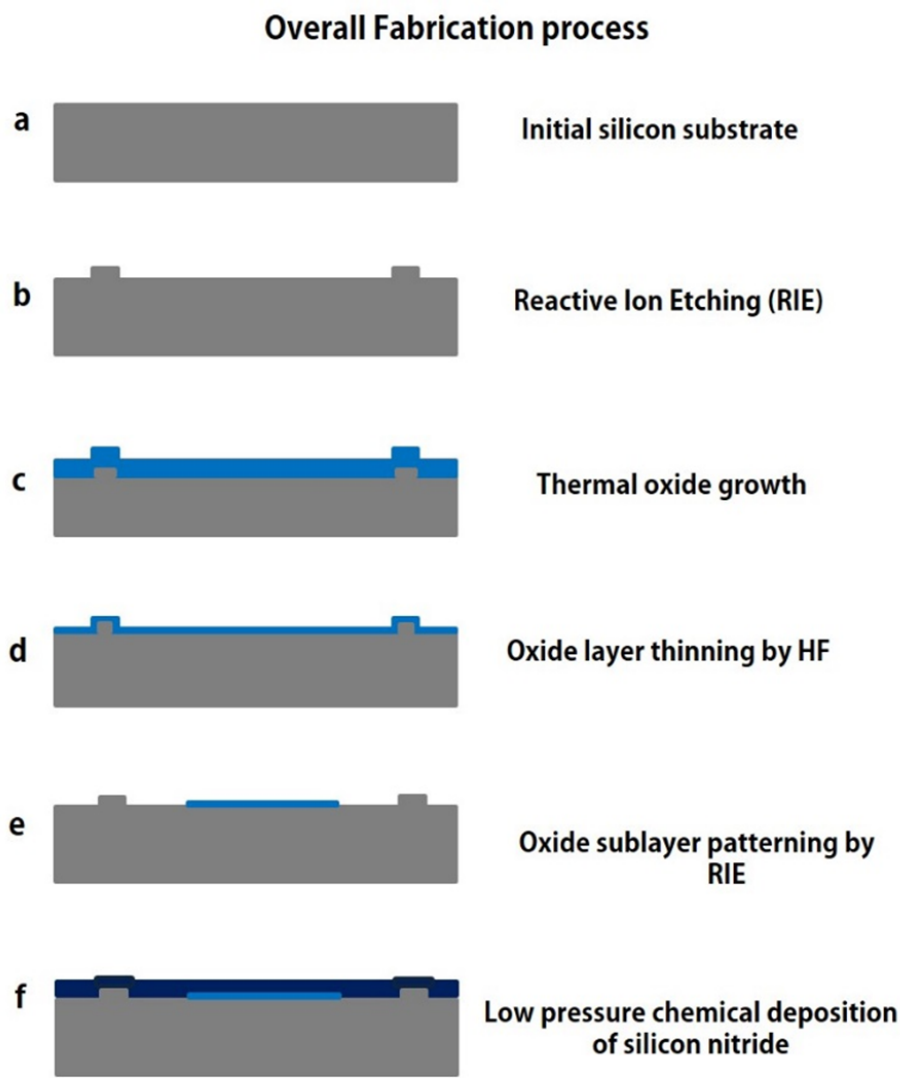

Figure 5. Process of predefined crack pattern. Notice the notch structures are employed to initiate nanocracks in anticipated direction. (a) Substrate preparation with standard wafer cleaning procedure. (b) RIE after photoresist patterning. (c) Thermal oxide growth if required (d) Oxide layer thickness control as required. (e) Oxide sublayer (buffer layer) patterning (f) LPCVD Si_3N_4 deposition.

2.2 Crack initiation and stop control

In order to fabricate various crack patterns including straight or oscillatory, a multi-layered cracking medium composed of Si_3N_4 or Si_3N_4 and SiO_2 is deposited on a Si substrate as illustrated in Figure 5. In such system, residual stress after deposition process induces tensile loading in the thin film.[24] Typically, this residual stress is released as unwanted cracks initiated by small amount of impurities incurred by edge beads during lithography. In order to prevent random cracking and controlled cracks occur selectively, an array of notch-like structures are employed as a stop structure which provides a deliberate collection of flaws, shown in Figure 6.

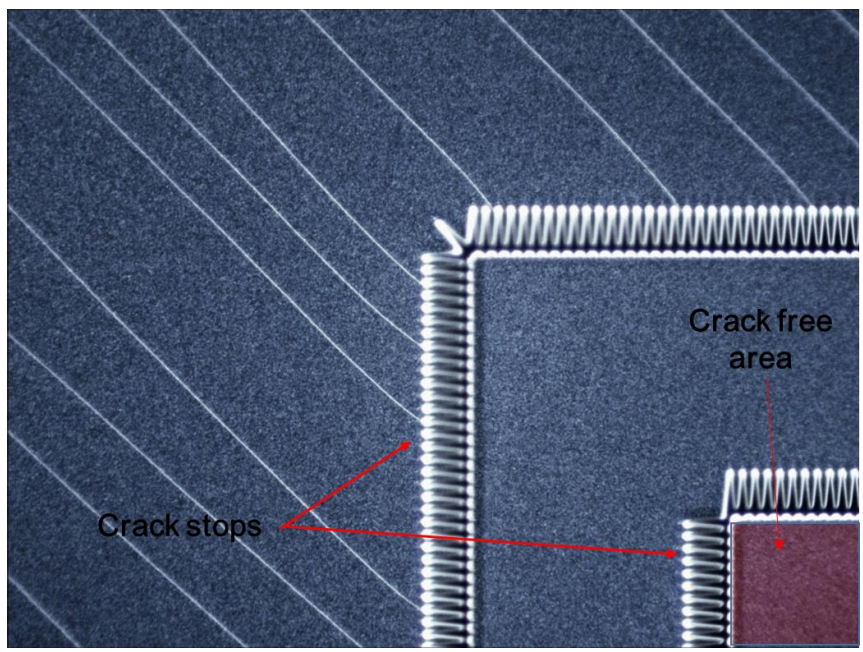

Figure 6. Crack stop structures and notch structure. Two rows of crack stop structures are employed to prevent cracks initiated from edge of the substrate coming into controlled crack region, colored as crack free area.

The notch structure, either embossed or engraved, also induces an acute stress concentration at the tip, provides an initial flaw for a crack to grow upon. As a result, a channeling crack is initiated to release the stored elastic energy in the Si_3N_4 thin film. In general, failure stress of through-thickness (channeling) cracks in an infinitely wide plate subjected to a remote tensile stress[25] which is governed by following equation: $\sigma_f = \sqrt{2E\gamma_s/\pi a}$, where σ_f is fracture stress, E is elastic modulus, γ_s is surface energy, and a is size of flaw. The notch tip serves as a flaw, **α**, thus the sharpness is an important parameter for crack initiation in the Si_3N_4/Si substrate system. In this study, no significant initiation rate increase is observed with 30˚ or smaller notch tip angle, therefore the notches with 30˚ tip angle is selected.

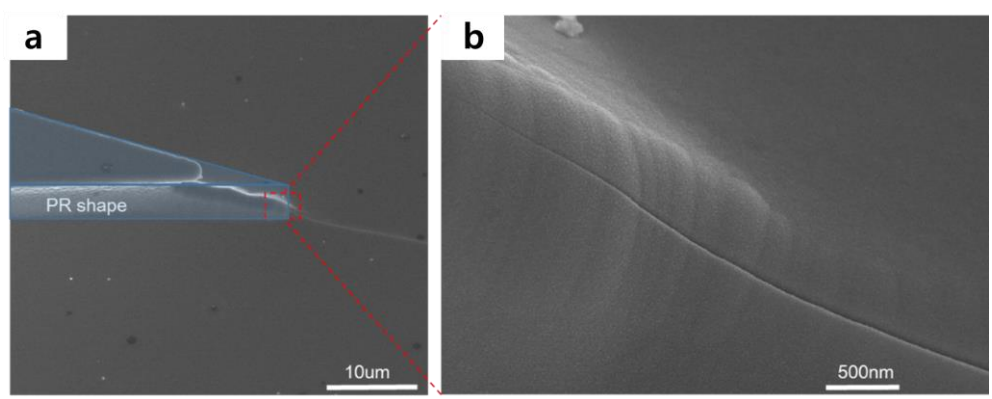

Figure 7. SEM image of a notch structure fabricated by dry etching process. (a) Initial photoresist shape shaded in blue and actual tip dulled by isotropic nature of dry etching (b) Magnified image of the tip showing an initiated crack.

Typically, the sharpness of the crack tip is affected by fabrication process, mainly by dry etching process. Locally increased etching rate at high aspect ratio features such as in the proximity of tip results in blunt shape as shown in Figure 7a as compared to the original photo resist shape indicated in blue color. Thus, the tip with more acute angle than 30˚ makes no difference unless etching method is changed. Since the cracks are successfully initiated with 30˚ tip angle, as shown in the blown up image, Figure 7b, no further study regarding tip sharpness and initiation rate is conducted.

2.3 Types of cracks

Once initiated, the cracks propagate in self-propagating manner. Unlike typical cracks found in other thin film/substrate system, Si_3N_4/Si system generates three major cracking types depending on the film deposition thickness. When the film thickness is under 800 nm, no cracks are initiated at the notch. Highly ordered cracks, oscillating with a specific amplitude and wavelength dominate in the Si_3N_4 thickness regime between 900 nm to 1500 nm while straight cracks are abundantly found in 800 nm to 900 nm thickness regime. As the film thickness is increased up to 1500 nm random cracking occurs. At 2000 nm, randomness of the cracks is substantially reduced at large scale, repetitive chain-like patterns are generated as shown in Figure 8.

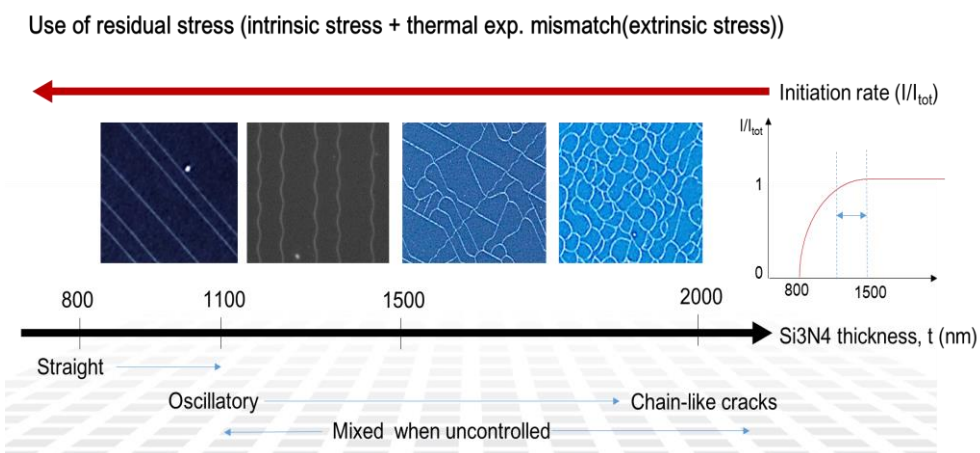

Figure 8. Major crack types found in Si_3N_4 / $Si_{(100)}$ system.

In a typical thin film/substrate system with an assumption that the film and substrate are elastically inhomogeneous, placed under plane strain

condition, and the substrate is substantially thicker than the film, G_{ss}, the energy release rate for steady state propagation of a channeling crack with substrate penetration[25] is governed by following,

$$G_{ss(material\ \#1)} = \frac{1}{h}\int_0^h G(a)da$$
$$G_{ss(material\ \#2)} = \frac{1}{a-h}\int_a^h G(a')da' \quad (1)$$

where G(a) is energy release rate at the crack tip. In general, G(a) is governed by relative film thickness to crack depth, stress, and elastic mismatch (α and β). The elastic mismatch[26] is expressed in terms of dimensionless parameters named as "Dundurs parameters,"

$$\alpha = \frac{E_1 - E_2}{E_1 + E_2},\ \beta = \frac{\mu_1(1-2v_2) - \mu_2(1-2v_1)}{2\mu_1(1-2v_2) + 2\mu_2(1-v_1)} \quad (2)$$

where $E_2 = E_2/(1-v_2^2)$ when subjected to plane strain condition, v_2, μ_2 are plane tensile modulus, Poisson ratio, and shear modulus substrate respectively. In case of the Si_3N_4 / $Si_{(100)}$ system, the elastic modulus and Poison ratio of Si (100) vary since the crystal structure of Si (100) is anisotropic[27]. Yet, no exact mechanism of oscillating crack in such system is discovered, it seems that the parameters listed in the equation (1) and (2) especially relative film thickness to crack depth and the anisotropy of

substrate material govern the propagation mode change in different film thickness regime.

In an attempt to clarify the effect of crystal structure of the substrate, as shown in Figure 9, various Silicon substrates having different crystal structure such as (100), (110), and (111) oriented Si substrates have been tested for oscillatory crack generation. Under identical experimental condition, the oscillatory cracks have not been discovered on (111) oriented Si substrates. On (110) oriented Si substrates, oscillatory modes are seldom found, however straight cracks predominantly occur unlike the Si (100) substrate case where major propagation mode is oscillatory.

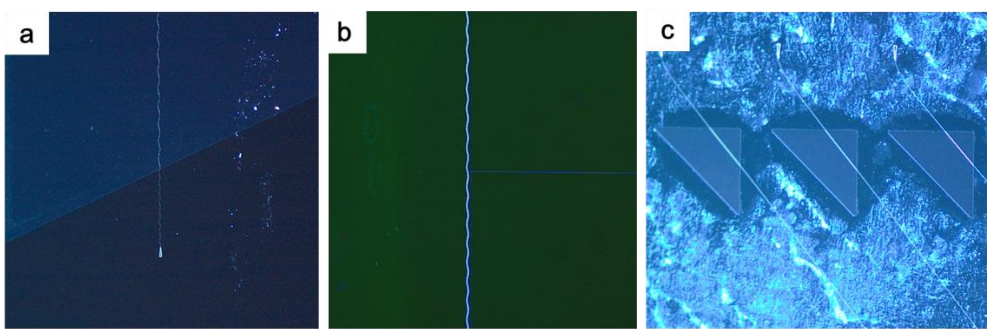

Figure 9. Different crystalline structure silicon wafer. (a) (b) (c) shows different Si substrate having crystallographic orientation (100), (110), and (111) respectively

2.4 Crack manipulation

The cracks demonstrated in this study self-propagate in steady oscillatory manner in [110] direction on (100) silicon substrate until it reaches the point where another stress concentration that surmounts the crack driving force.[28] Although the exact cause of the oscillation is yet clearly defined, it appears to be related to the crystal structure of underlying silicon substrate and applied stress.

Increased film thickness of Si_3N_4 leads to higher stored elastic energy in the Si_3N_4/Si system, in turn shorter wavelength oscillatory cracking occurs. As shown in Figure 10b, the wavelength can be increased by reducing Si_3N_4 film thickness. In terms of energy, an oscillatory crack creates more surface area per unit area of the substrate thus releases more energy than a straight crack with an assumption that the depth of the penetration is equal. In addition, it is well known that the surface energy of crystal silicon varies with cleavage plane[29]. This is related to the number of broken bonds by fracture. The number of broken bonds increases in the order of {111}, {110} and {100} plane, and the number ratio is known to be $1:(3/2)^{(1/2)}:3^{(1/2)}$, therefore the fracture energy (~2·surface energy, γ_{hkl}) is the highest for {100} and the lowest for {111} plane[29]. As mentioned earlier, the crack penetration into Si (100) substrate for the straight crack is in {111} plane as opposed to the oscillatory crack which has the penetration angle altering within {111} in relation with phase of the oscillation. Therefore,

under higher energy state (typically the thickness of silicon nitride film is greater than 0.9μm), oscillatory cracks prevail as opposed to straight cracks which occur under relatively low energy state[30].

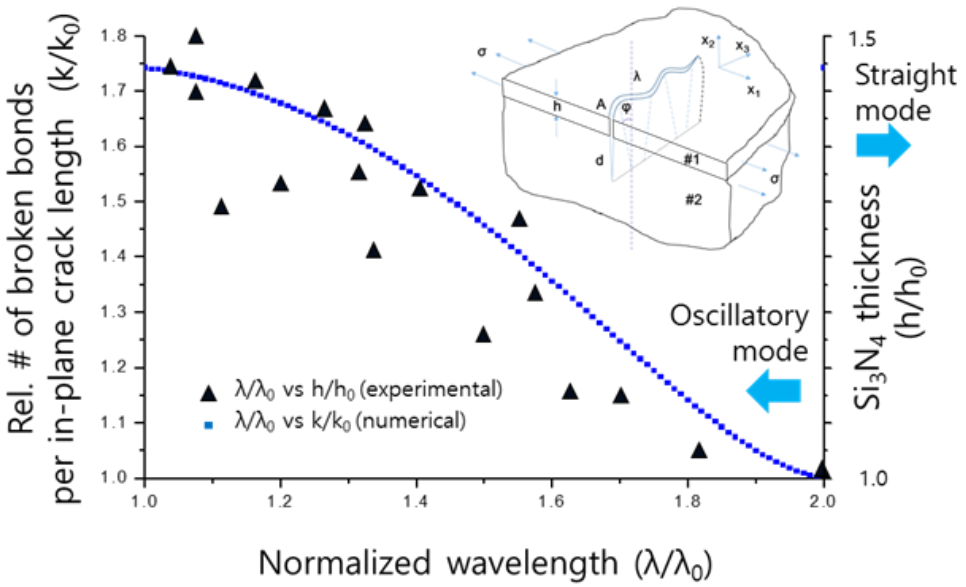

Figure 9.2. Experimental result plotted over numerically calculation value of equation (3).

Assuming a typical oscillatory crack follows sine wave equation, $x_1 = A \sin(2\pi x_3/\lambda)$, where x_2 is in-plane propagation direction of the oscillatory crack, x_3 is depth direction. The relation between number of broken bonds and film thickness, h, can be expressed in terms of amplitude, A, penetration depth, d, wavelength, λ and surface energy of silicon substrate, γ which depends on the angle of penetration, φ as following,

$$K \sim \frac{1}{\lambda}\int_0^{\lambda}\left[A^2 \cdot \sin\left(\frac{2\pi x_3}{\lambda}\right)^2 + d^2\right]^{1/2} \cdot \gamma_{s\,(\varphi)}\, dx_3 \qquad (3)$$

The equation (3) shows number of broken bonds are weighted by the wavefunction and the depth. The numerical result is shown below. As shown, the experimental data plotted in triangles well matches numerically calculated value thus simple theory based on number of broken bonds and wavelenth is verified.

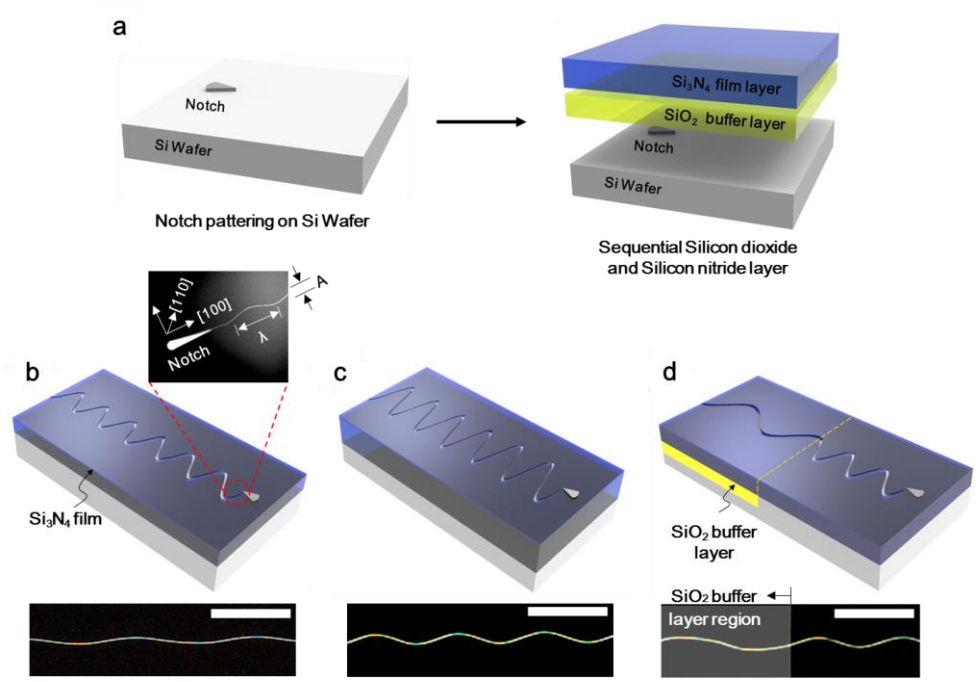

Figure 10. Schematic diagram of crack generation. (a) Structure of nanocrack (b) An oscillatory crack generated on Si_3N_4 film with propagation direction in [110] on (100) silicon wafer and its corresponding optical microscopic image with a 100μm scale bar. (c) Manipulated wave property within the SiO_2 buffer later region.

The simplest method for manipulating the oscillatory cracks in Si_3N_4/Si film-substrate system is to regulate the Si_3N_4 film thickness which constitutes the amplitude and wavelength simultaneously, shown in Figure 10c. As the Si_3N_4 film thickness is increased, the amplitude of the oscillatory cracks is substantially increased as shown in Figure 10b and 10c. Regulating film thickness simultaneously changes the wavelength and the amplitude. Figure 10d shows the transition of wavelength at the interface of composite film (made of SiO_2 and Si_3N_4) and typical Si_3N_4 film. The transition from oscillatory mode to straight mode also occurs when the crack propagates over thinner silicon nitride film as shown in Figure 11b due to the stored elastic energy reduction by reduced Si_3N_4 film thickness.

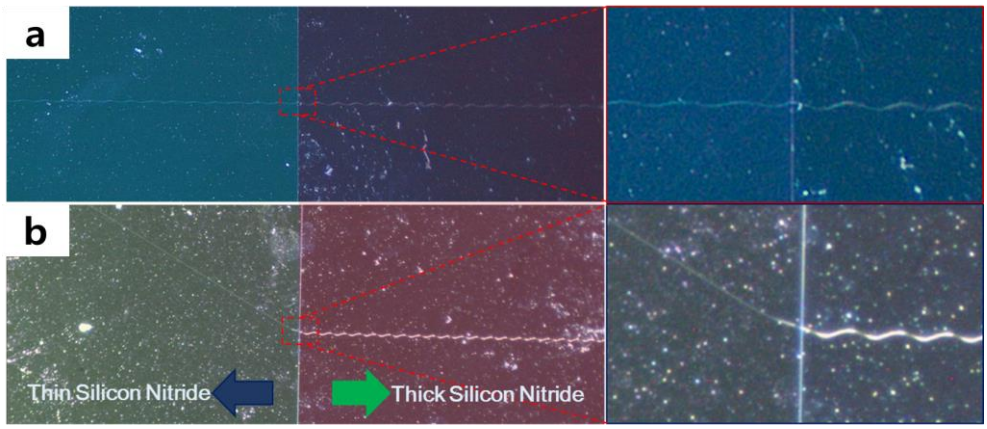

Figure 11. Manipulation of oscillatory crack by Silicon Nitride thickness. (a) Wavelength of an oscillatory crack is decreased as propagating over different thickness regions. (b) Propagation mode is changed from straight to oscillatory as propagating from thinner silicon nitride region to thicker region (from left to right).

In order to manipulate the wavelength separately from amplitude of an oscillatory crack, a SiO_2 buffer layer is employed between Si substrate and Si_3N_4 thin film. As shown in Figure 10d, the wavelength of the oscillatory crack is considerably increased by the buffer layer with negligible amplitude difference.

The oscillatory cracks accompany a substantial substrate penetration (approximately 3 um) in altering angle as opposed to the straight crack which has penetration angle in {111} plane only. Since the alteration of penetration angle requires higher fracture energy as discussed earlier due to number of broken bonds, it is obvious that the oscillatory cracking mode is preferred under higher energy state. This matches our experimental result, discussed in the later chapter, showing that increased Si_3N_4 film thickness, meaning higher stored elastic energy state, leads to shortened wavelength of oscillatory cracks while amplitude is increased. When the Si_3N_4 film thickness is increased even more, catastrophic cracking occurs as shown earlier in Figure 4d where no straight cracks are found. In addition, the kinking of the cracks is extremely radical in this Si_3N_4 film thickness regime.

The SiO_2 buffer layer generates similar effect as reduced Si_3N_4 thickness on the cracks. Thermally grown SiO_2 film on the Si substrate is known to generate compressive stress which is the opposite of Si_3N_4 film's residual stress. In addition, the buffer layer changes elastic mismatch between the film and substrate in reducing elastic energy of the film/substrate system. As a result, tensional stress is reduced thus

wavelength of an oscillatory crack is increased as the buffer layer thickness is increased.

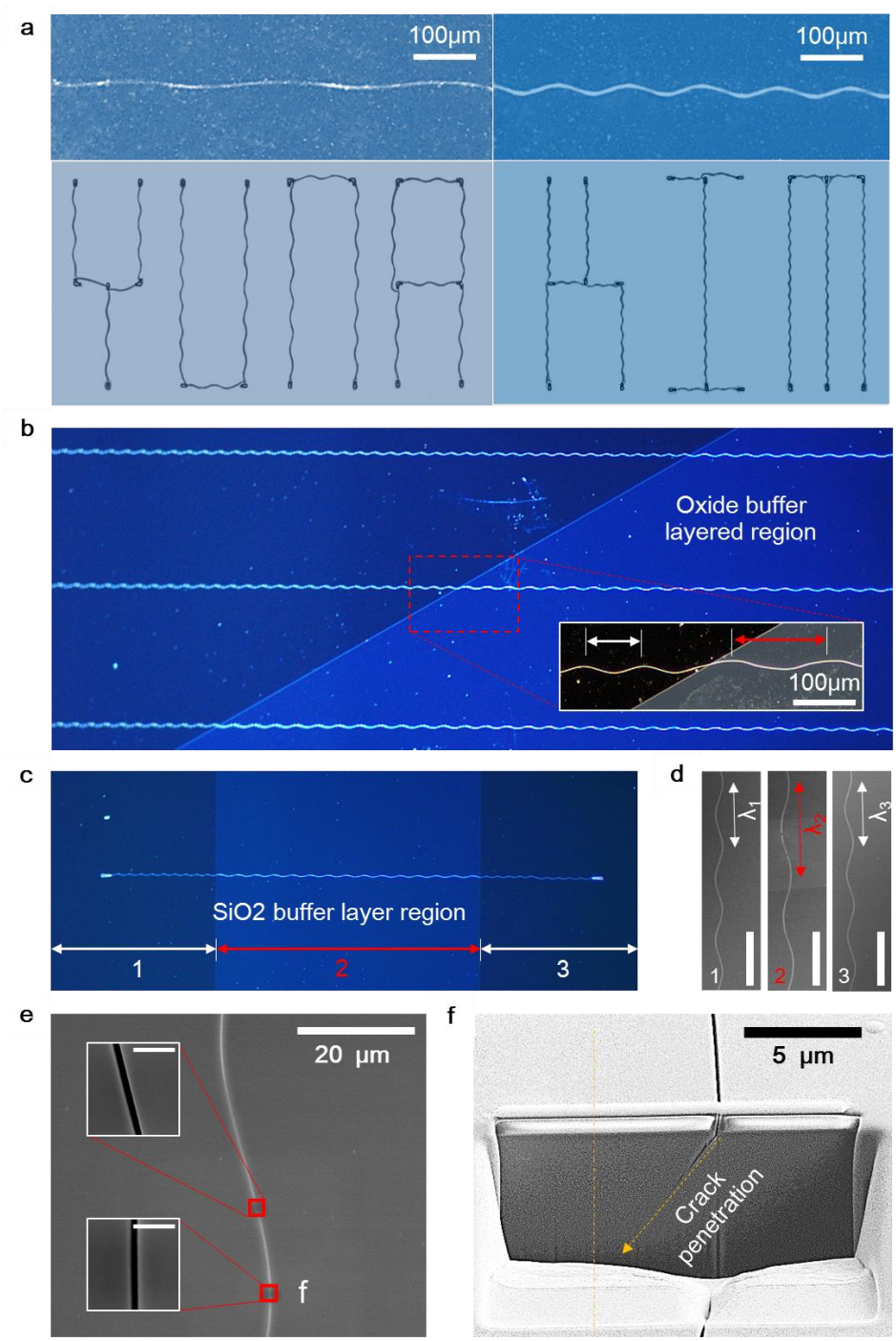

Figure 12. Representative image and magnified SEM image. (a) Oscillatory

cracks with different amplitude and wavelength using different Si_3N_4 film deposition thickness and underlying buffer layer. (b) An array of high aspect ratio nanopatterns each of which having nanoscale width and centimeter scale length. (c)-(d) An oscillatory crack is initiated and stopped. The wavelength of the oscillatory cracks is significantly increased in the silicon dioxide buffer layer region, and corresponding SEM images of the region 1, 2, and 3 are shown. Scale bar: 100 μm. (e) Width of a typical oscillatory crack. Inset scale bar: 1 μm (f) Section image of an oscillatory crack in depth direction obtained via FIB.

Complementary use of the Si_3N_4 film and silicon oxide buffer layer enable manipulation of two major properties of the oscillations: wavelength and amplitude, separately. Top left image of Figure 12a (left) shows an oscillatory crack generated on 900 nm Si_3N_4 film with 50 nm SiO_2 buffer layer. The wavelength of the oscillatory crack is ~200 μm, and the amplitude is roughly 1/20 of the wavelength. On the contrary, wavelength of the oscillatory cracks found on 1.2 μm thick Si_3N_4 film without buffer layer is approximately 100 μm and the amplitude is roughly 1/10 of the wavelength as shown in Figure 12a (right). This shows that simultaneous use of specific Si_3N_4 film thickness that corresponds to target amplitude and the SiO_2 buffer layer provides a utility for wavelength and the amplitude control.

Selective etching of buffer layer prior to the Si_3N_4 film deposition

enables localized control of wave properties as shown in Figure 12b and 12c. When an oscillatory crack propagates over the patterned SiO_2 buffer layer region, the wavelength of the oscillatory crack is increased beginning at the interface whereas amplitude remains unchanged. In Figure 12b, multiple oscillatory cracks are generated by placing a notch array in parallel manner. Inset of Figure 12b confirms prominently increased wavelength of an oscillatory crack as propagating over the patterned SiO_2 buffer layer area (triangular shape). Unless there are stress constraints such as defects or other structures including crack stop or notches, the cracks propagate continuously in the buffer layer region in the same way as the propagation in non-buffer region.

This wavelength manipulation is reversible. Once increased wavelength can be decreased via patterning the SiO_2 buffer layer as shown in Figure 12c. The oscillatory crack initiated from a notch has initially shorter wavelength until the crack reaches the SiO_2 buffer layer interface. As the crack passes the interface, the wavelength is elongated. Inversely, as the crack leaves the buffer layer region, the wavelength is decreased back to the initial value. Corresponding scanning electron microscope (SEM) images of the oscillatory crack in each regions confirm locally increased wavelength in the buffer layer region, shown in Figure 12d.

The silicon oxide buffer layer has an insignificant or small effect which is extremely difficult to measure on the width of the cracks. Figure 12e shows the width of a typical oscillatory crack which is approximately

120~150 nm. Although there are slight variations depending on the location or geometry of structures near the cracks, it appears that the width of the oscillatory cracks in SiO_2 buffer layer region is 100 to 150 nm which is not considerably different than that of non-SiO_2 region.

Although a linearly increasing trend in width of cracks initiated on substrates with different film thickness is not determined in this study, there likely be a connection between the crack width and film thickness. Within a whole 4" Si (100) substrate, considerable crack width variation, 120nm ~150nm, caused by the defects or non-uniform stress field which is originated from unwanted cracks initiated especially at the edge of Si substrate, is observed. Although the crack stop structure prevents these unwanted cracks extending in controlled region as shown in Figure 13a, the initiation and total number of these cracks cannot be perfectly controlled, therefore the stress field of a wafer to another cannot be uniform. Nevertheless, we were able to initiate an oscillatory crack over a region where two different Si_3N_4 film thickness is adjacent as shown in Figure 13b. In this way, we were able to compare the width variation due to film thickness within a localized region where effect of stress non-uniformity is minimized. The width of shorter wavelength crack which corresponds to the thicker Si_3N_4 film (approx. 12000 Å) is 170nm and the width of longer wavelength crack which corresponds to thinner Si_3N_4 film (approx. 8000 Å) is 90nm. Again, this result is limited to relative width variation case only.

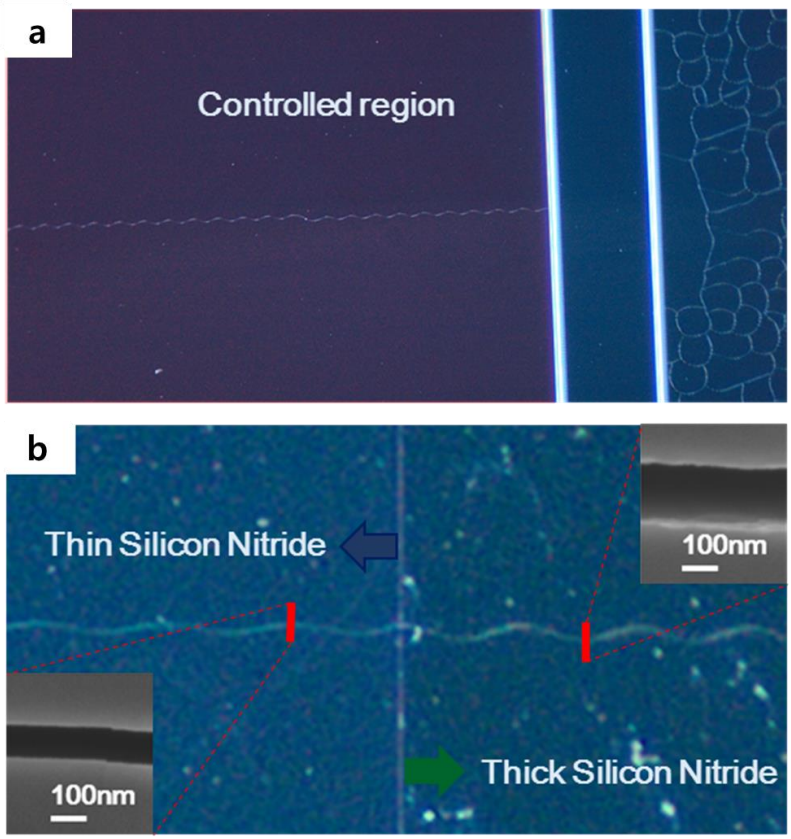

Figure 13. Optical microscope images of controlled cracking and single oscillatory crack propagated over different Si_3N_4 film thickness (a) Optical microscope image of crack stops constructed for controlled cracking region. The silicon nitride (Si_3N_4) thickness of this sample is approximately 1.6 um. (b) Wavelength manipulated by different thickness silicon nitride deposition. Inset images show SEM image of an oscillatory crack propagated on different film thickness. The film thickness of each region is 800nm and 1200nm.

In any cases of the oscillatory cracks, significant substrate damage through the thickness direction is accompanied. This penetration of the

crack into the Si (100) substrate is much deeper than the thickness of the Si_3N_4 thin film due to high elastic energy of the Si_3N_4 film and relatively compliant Si substrate.[31] The crack tip in depth direction seems to conform to center line of in-plane propagation direction which coincide with [110] direction on (100) oriented Si substrate. The penetration length is related to the amplitude since the maximum slope of the penetration into the substrate is always inwards toward to in-plane propagation direction of the oscillatory crack. It appears that the maximum penetration angle occurs at the peaks of the wave and the corresponding angle coincides with (111) plane of the Si (100) substrate as revealed in focused ion beam (FIB) section image shown in the Figure 12f. As the oscillatory crack completes one cycle of sine wave, the penetration angle rotates from approximately 55˚ to -55˚ degrees with respect to center of axis which coincides with in-plane propagation direction of the oscillatory crack.

In the Si_3N_4/Si film-substrate system, initiation rate of the oscillatory crack as well as straight crack significantly increases as the film thickness, h, increases since the thicker Si_3N_4 film results in higher stored elastic energy in the system.[31] All cracks including random and oscillatory form are rarely found when the h is less than 900 nm because insufficient amount of stored elastic energy for the initiation is established whereas initiation rate is greatly improved where h is increased to near 1.1 μm. Similar to the initiation rate, amplitude is related to the Si_3N_4 film thickness. As shown in Figure 13a, the amplitude of the oscillatory crack has a proportional

relationship with the Si_3N_4 film thickness although there are some uncertainties due to unintended structures such as defects.

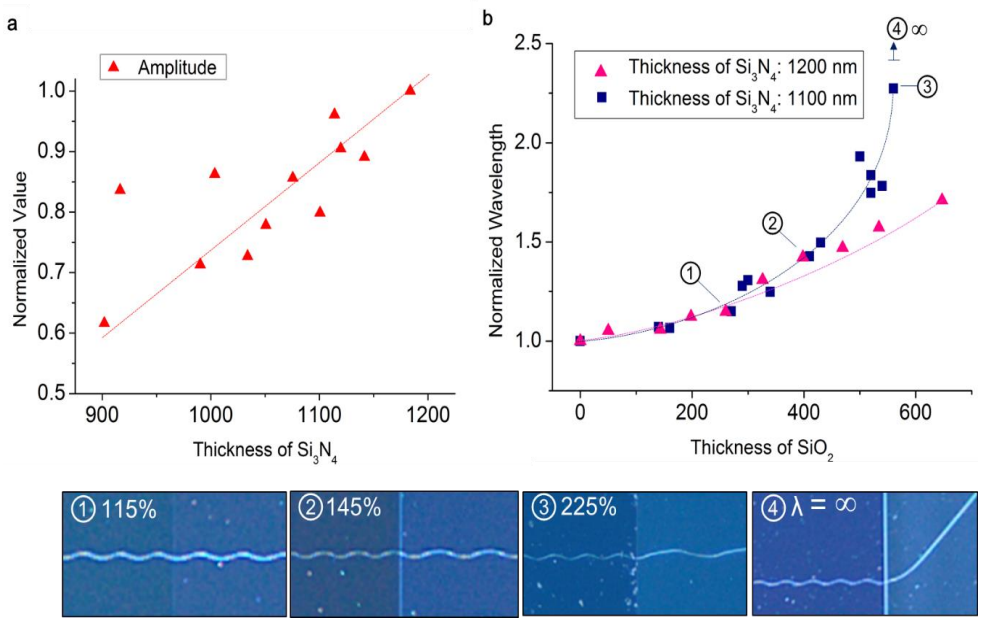

Figure 14. (a) Normalized wavelength and amplitude of the oscillatory cracks plotted against different Si_3N_4 deposition thicknesses. (b) Normalized wavelength of the oscillatory cracks plotted against SiO_2 buffer layer thickness and corresponding optical microscope images of oscillatory cracks.

In order to independently control the wavelength from the amplitude and to have the film thickness fixed at optimized value for highest oscillatory crack initiation, additional thin film layer is employed under the Si_3N_4 film. This material has to meet two qualifications: compatibility with micro fabrication process and no significant total thickness increase. SiO_2 meets these requirements. The SiO_2 buffer layer promotes favorable effect on the given system with relatively small increase in the overall thickness of

the Si_3N_4/SiO_2 multi-layered thin film.

The range of this additional layer thickness required for wavelength manipulation is up to 1000Å which is relatively small as compared to 1.1 μm of Si_3N_4 film thickness at optimal initiation rate. As shown in Figure 14b, the SiO_2 buffer layer thickness under 700Å is sufficient to convey wavelength increase up to 225% while the amplitude change, which is primarily governed by the film thickness, is restrained. It appears that this phenomenon is related to elastic mismatch between the film and the substrate.[32] The wavelength of the cracks has exponential relationship with the buffer layer thickness as shown in Figure 14b. When the SiO_2 buffer layer thickness is greater than 700Å, oscillatory propagation mode turns into straight mode. When the Si_3N_4 film thickness is reduced, wavelength increase rate per unit SiO_2 buffer layer thickness is also increased. The result shown in Figure 14b indicates that the wavelength increase rate surges with reduced Si_3N_4 film thickness.

2.5 Complex nanopattern fabrication by crack manipulation

Complementary use of SiO_2 buffer layer with various patterns and thickness enables wavelength manipulation and fabrication of unique nanopatterns which is difficult to fabricate through conventional nanopatterning processes especially in large area. As shown in Figure 15a, the wavelength of an incident wave becomes elongated in the SiO_2 buffer layer region as if the wavelength of an optical wave is increased when it propagates through a medium with lower refractive index. Refraction of an oscillatory crack which is comparable to that of optical wave can also be attained. As shown in Figure 15b, the propagation direction and mode can be manipulated by employing a SiO_2 buffer layer. The buffer layer with thickness greater than 70nm changes oscillatory propagation mode to straight mode. At the in-plane interface of SiO_2 buffer layer, the incident oscillatory crack kinks to conform to straight crack's principle propagation direction. As a result, the in-plane propagation direction is changed from [110] to [100], which are the principle propagation directions of the each modes on (100) Si substrate, respectively. This propagation mode and direction change is invertible since the exactly opposite phenomenon occurs as the straight crack leaves the buffer oxide region. As shown in the cross section image attained using FIB, the straight crack in the SiO_2 buffer layered region has penetration angle similar to that of oscillatory crack at the incident phase, Figure 15c. This indicates the incident penetration angle

is maintained throughout the propagation in the SiO2 buffer layer region, thus the phase of incident wave at the interface determines the in-plane kinking direction.

At an arbitrary phase of the oscillatory crack, corresponding penetration angle with respect to the principle propagation axis of the oscillatory crack always lies between -55˚ and 0˚ or +55˚ and 0˚. For simplicity, positive phase which is right hand side with respect to the principle propagation axis of the oscillatory crack from the view point towards crack tip is defined as right hand phase (RHP) and the opposite is defined as left hand phase (LHP). When the phase is in RHP range, the penetration angle is also in the positive range. In such case, the crack kinks to the left at the interface, and vice versa as shown in Figure 15d. Similarly, when the crack exits the buffer layer region, the straight crack is transitioned to the oscillatory crack. The straight crack's penetration angle does not exceed its maximum angle of 55˚, and the penetration angle of the incident phase is maintained. When the straight crack exits the buffer region, it kinks to the opposite direction as the penetration angle begins to oscillate again between -55˚ and +55˚ and the propagation mode transition from straight to oscillatory occurs. In order to successfully control kinking direction, wavelength control is crucial in terms of anticipating the exact path of the propagation and of realizing elaborate crack patterning.

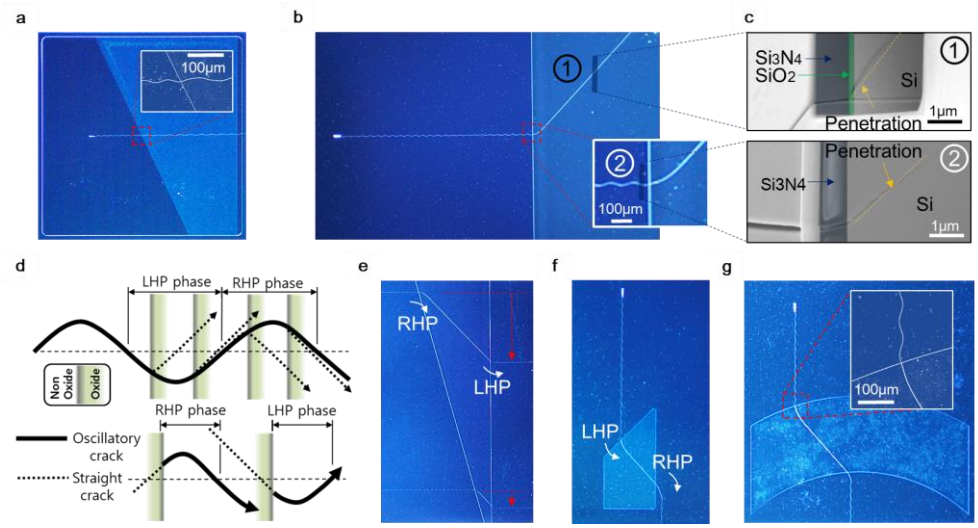

Figure 15. Selection of crack direction. (a) Wavelength elongation by thin SiO_2 buffer layer. (b) Propagation mode changed from oscillatory mode to straight mode by thick SiO_2 buffer layer. (c) Cross section (FIB) image of straight (top) and oscillatory (bottom) crack. (d) Selection of crack kinking direction when oscillatory crack impinging into SiO_2 buffer layer region (top) and when straight crack exits the SiO_2 buffer oxide region (bottom) (e) propagation shifted by straight crack travel distance (f) Propagation shifted leftward direction using SiO_2 buffer layer (g) Propagation direction manipulated by SiO_2 buffer layer patterned like an optical lens.

Using these wave-like properties of the oscillatory crack with elaborate control of incident phase and the incident angle at in-plane interface of SiO_2 buffer layer, various manipulations can be achieved, propagation shift for instance. Figure 15e shows selective shift of the two waves by adjusting propagation length of straight portion. The propagation

shift in opposite direction can also be attained as shown in Figure 15f. When the incident angle between the oscillatory wave and the interface is properly controlled, the cracks can be focused into a specific location as if optical wave is focused by lens as shown in Figure 15g.

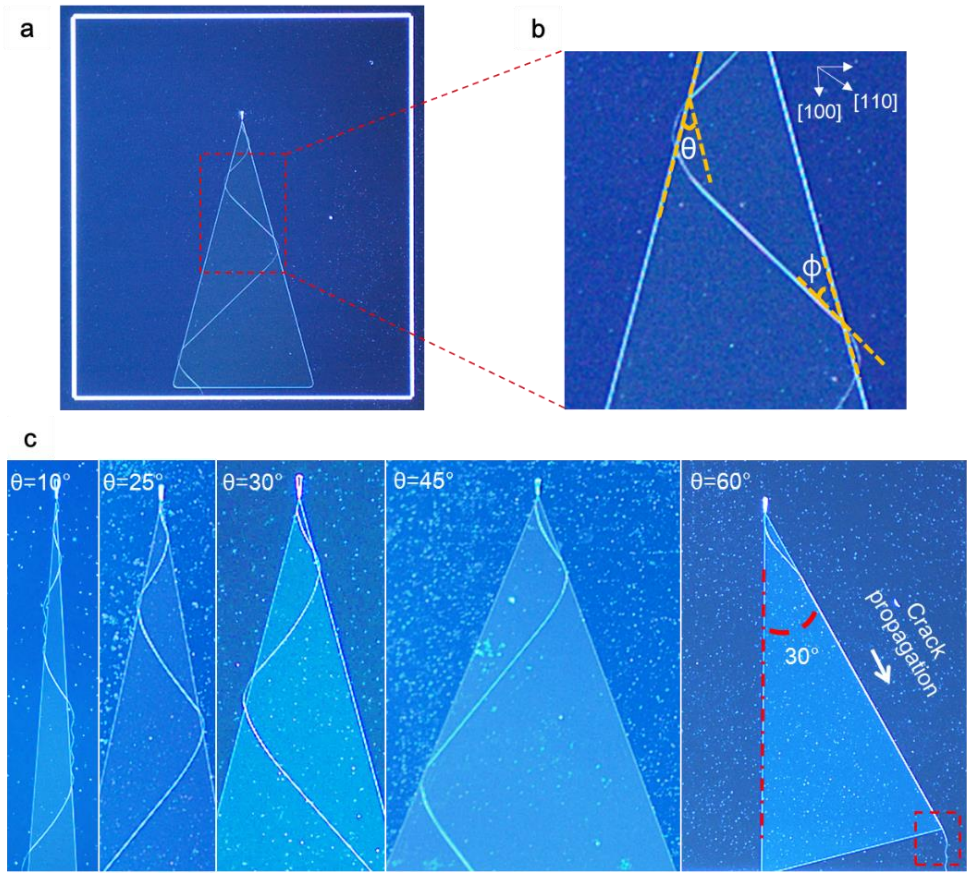

Figure 16. Amplification of oscillatory crack. (a)-(b) Representative optical image of amplified oscillatory crack and its enlarged area. (c) Images of ascending amplification of the wave by differing angles of the buffer SiO_2 pattern and the crack propagated along the interface.

Another wavelike properties of oscillatory crack include

amplification, total internal reflection (TIR), and evanescent wave. Using these properties enables fabrication of interesting patterns over large area. By placing a triangular shape SiO_2 buffer layer with an apex facing a notch tip, an initiated crack meanders two adjacent sides of the triangle due to refraction at the edges of the triangle as if total internal reflection of optical wave. In terms of amplitude, this can be seen as amplification. The degree of amplification is governed by the angle of apex, θ. As shown in Figure 16b, the angle ϕ, between the interface and the crack tip determines the final propagation direction of the crack. When ϕ is sufficiently large (>15˚), the crack kinks back into the buffer layer region and starts propagating to the opposite direction. As this process is repeated, unique nanopatterns are fabricated as shown in Figure 16a. When the crack tip angle coincide with the boundary of the SiO_2 buffer layer region where ϕ is <15 ˚, the crack propagates along the edge of the buffer layer. Despite the principle propagation direction of the straight crack is [110] on (100) Si wafer, the straight crack propagates along the edge as shown in Figure 16c. This phenomenon resembles evanescent wave of optical wave.

2.6 In-situ patterning using laser indentation process

Similar to initiation of cracks by surface geometry of thin film, an acute stress concentration can be generated by focused laser beam. As illustrated in Figure 16.1, pulsed UV laser @314nm generates enough energy to ablate the Si_3N_4/Si film substrate system. The holes that coincide with the spot size of the beam made by laser ablation of Si_3N_4/Si works as crack initiator similar to the notch structures demonstrate in the earlier part of this study. The setup of optics and initiation process is illustrated in Figure 16.1.

The initiation rate of steady state crack propagation can be controlled by laser power and the scanning length. The laser power governs the depth and size of the initial ablated holes as well as the sharpness along the perimeter of ablated area. As shown in Figure 16.2, as the laser power is increased, the substrate damage is increased. For a thin film crack to propagate steadily with substrate penetration in Si_3N_4/Si system, at least 3-4 times the Si_3N_4 film thickness is must be accompanied. The Si_3N_4 film thickness used is approximately 800 nm thus penetration depth must be deeper than 4-5 um. With low power of laser, sufficient depth cannot be attained.

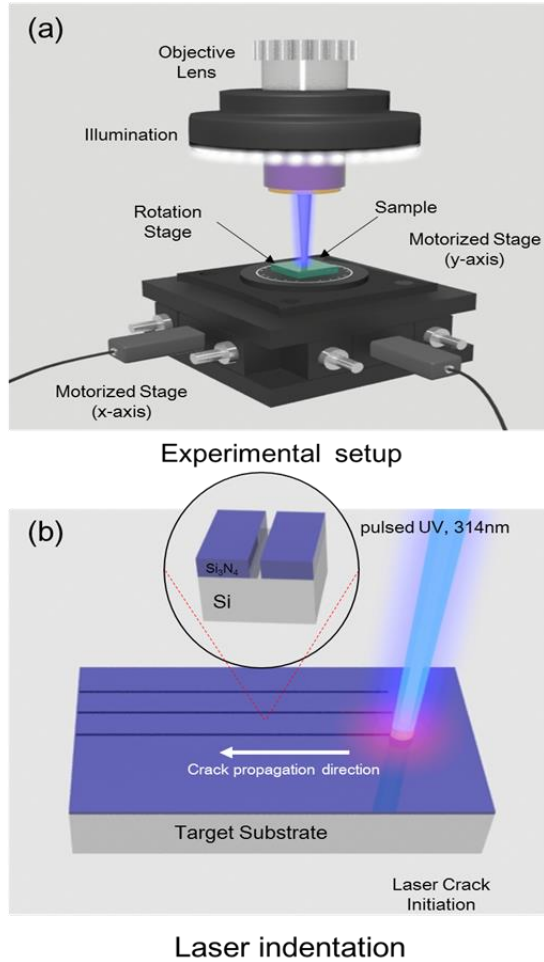

Figure 16.1 Cracks initiated by laser indentation process. (a) Experimental setup and (b) blown up image of typical generation of crack propagation on Si_3N_4/Si system.

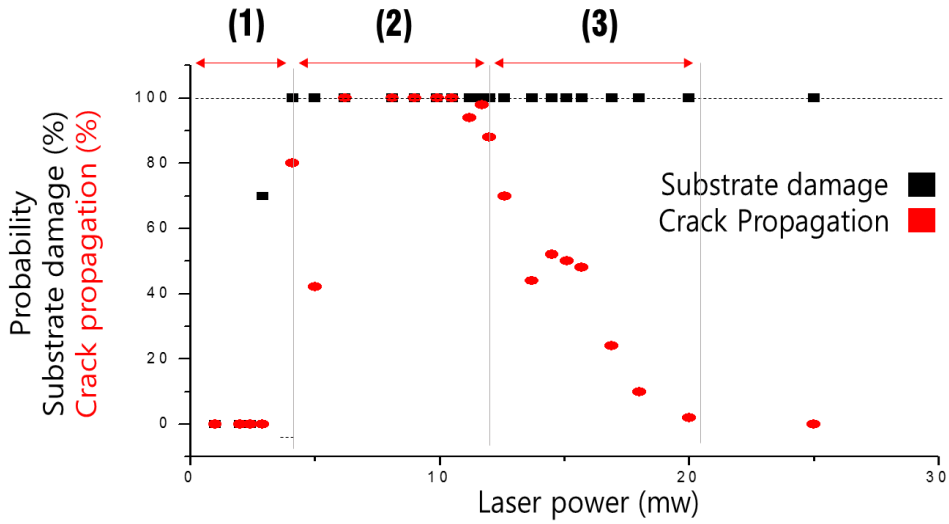

Figure 16.2 SEM image of ablated hole and extension of scanning to create steadily propagating crack.

The minimum power required for ablation of Si substrate is experimentally found to be 5 mW. As shown in Figure 16.2, in the region (1), where laser power is less than 5 mW, the Si_3N_4 is film is selectively ablated and no substrate penetration is accompanied. In the region (2), significant damage into the substrate is achieved. The depth of damage into the Si substrate is similar to a typical crack's penetration depth made using notch like structures, ~4-5 um, in corresponding Si_3N_4/Si system. In this power regime, probability of steady state crack propagation is the highest. When the laser power exceeds 10 mW, the penetration depth is far deeper than the typical penetration depth and the edge roughness along the perimeter of the ablated hole is greatly reduced. As a result, the stress concentration effect is

reduced thus steady state propagation is not achieved unless higher stored elastic energy is induced.

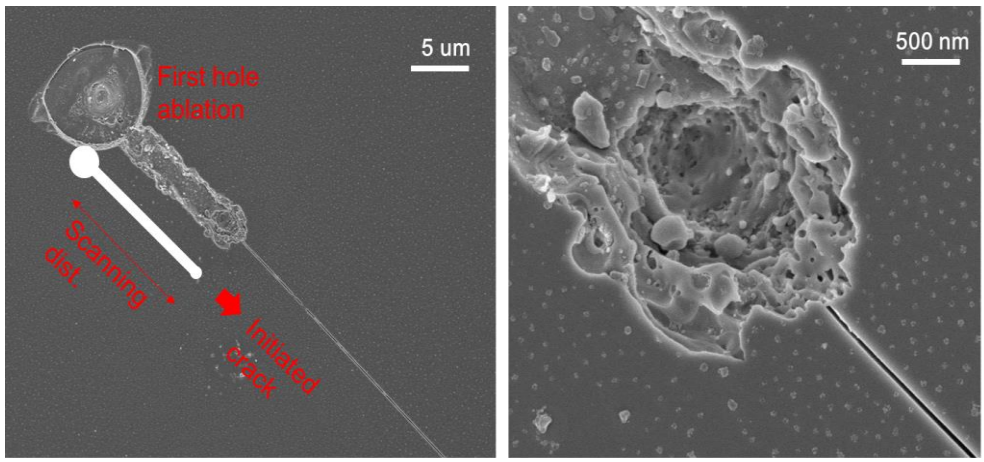

Figure 16.3 SEM image of ablated hole and extension of scanning to create steady state crack propagation.

Another important parameter for initiation of steady state crack propagation by laser indentation is the scanning length. For a film crack to propagate in steady state, it is known that the initial length or size of the defect must be at least twice the depth of the crack[33]. In the Si_3N_4/Si system, the Si substrate is much more compliant than the Si_3N_4 film, thus crack always penetrates into the substrate. The penetration depth as shown in the earlier part of this study is approximately 4-5 um, thus it can be inferred that the indentation length in in-plane direction must be greater than ~10um. (ref. hutchson) As shown in Figure 16.3 (left image), additional scanning after ablation of initial hole in plane direction of the crack propagation direction enables steady state propagation of a crack.

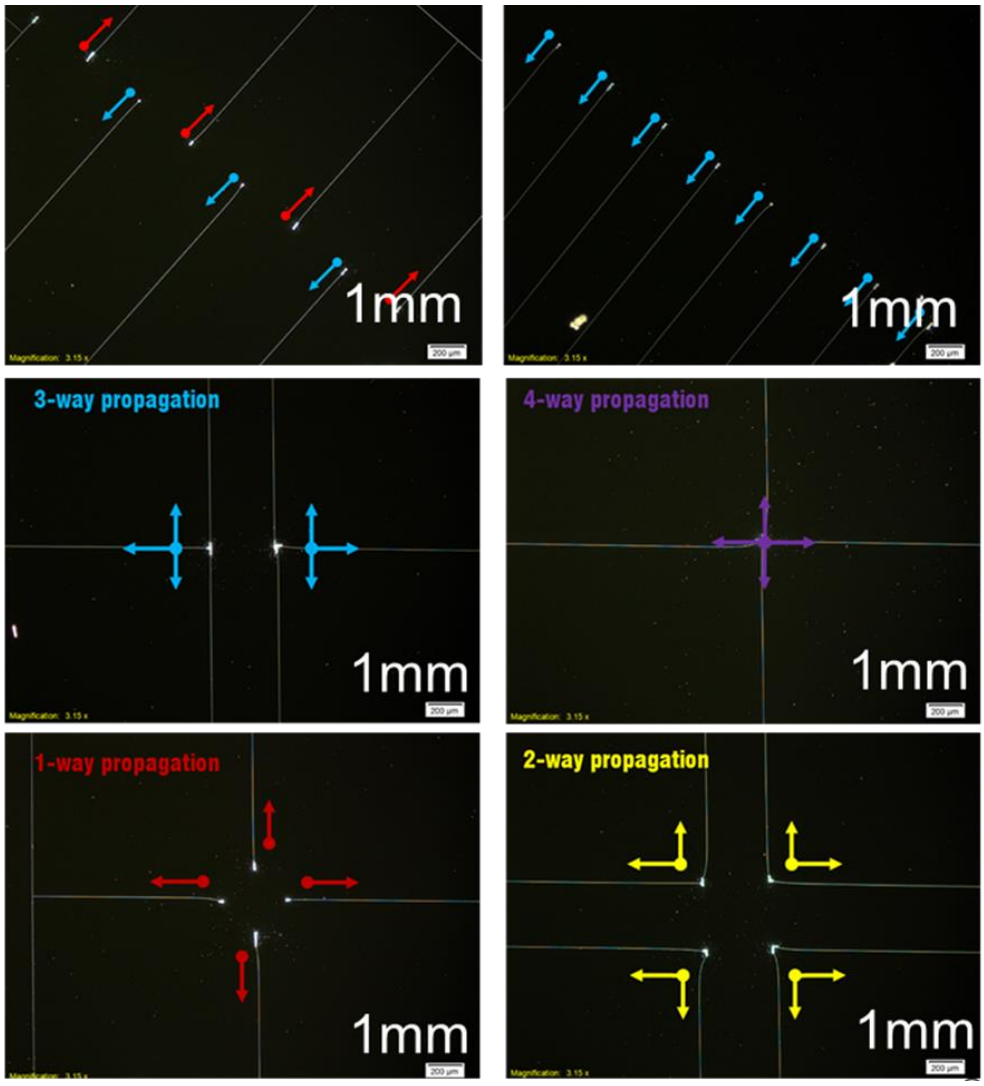

Figure 16.4 Advanced pattern fabricated using laser indentation process. Notice line width of all cracks is under 100 nm.

Using initiation of steady state crack propagation by laser indentation, various patterns can be fabricated. The cracks made in this manner have less than 100 nm width unless Si_3N_4 film thickness is increased from 800 nm which is typically used in the laser ablation process. As shown in Figure 16.4, arrays of nanocracks in altering directions or

unidirectional nanocracks are fabricated. By changing scanning directions from a single ablated hole, multidirectional (up to 4 directions) cracks can also be made. The propagation of the cracks are continuous unless a crack stop is placed, thus it is advantageous to fabricate a large scale nanopattern which is very difficult to obtain using conventional lithography technique.

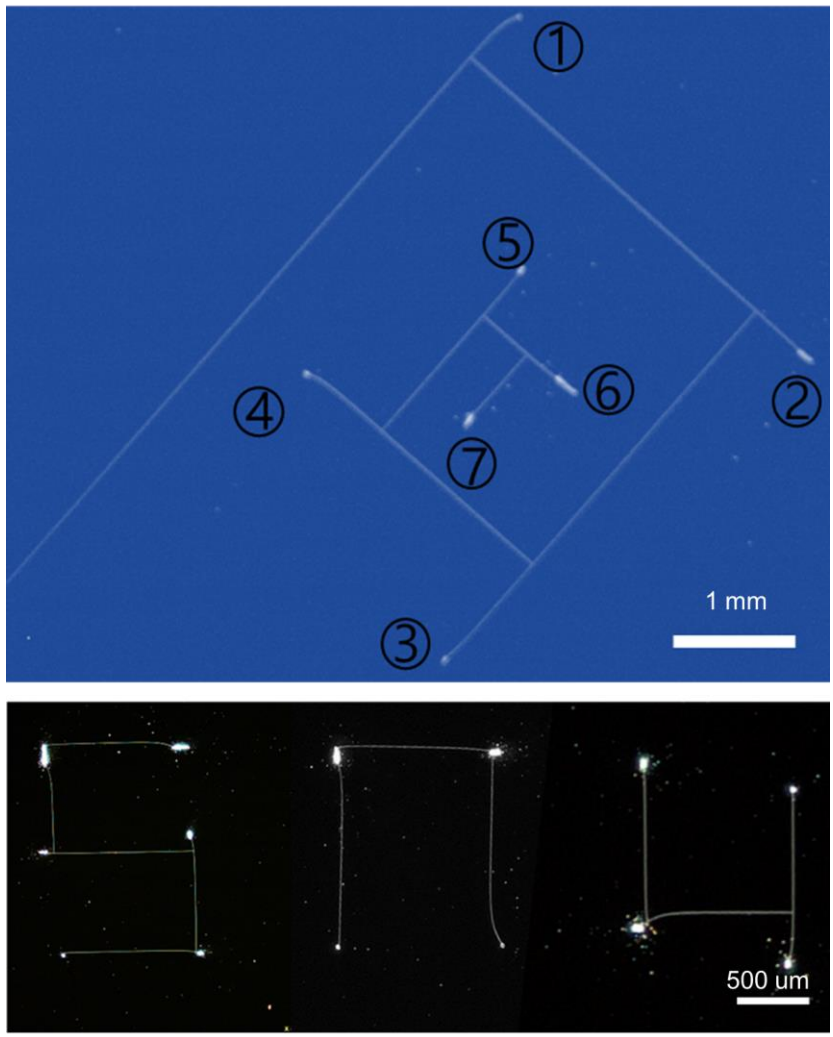

Figure 16.5 Advanced pattern fabricated using laser indentation process. Notice line width of all cracks is under 100 nm.

Simultaneous use of ablated sites and existing cracks provide a fine utility for complicated pattern fabrication. A typical crack itself works as a crack stop since the crack provide a discontinuity in the cracking medium. Similarly, the holes created by ablation or ablated sites can work as a crack stop since the cracking medium (Si_3N_4 film) removed. Without a cracking medium, no cracks can propagate, thus ablated holes or sites can be used as a crack stop. Using existing cracks and ablated sites simultaneously, a maze like pattern and letters (SNU) can be fabricated as shown in Figure 16.5. The width of such cracks are all in nanometer scale, ~100 nm or under. The finer linewidth can be attained by employing thinner Si_3N_4 film as a cracking medium as discussed in earlier part of this study. The tradeoff is the initiation rate of the cracks since the stored elastic energy is reduced.

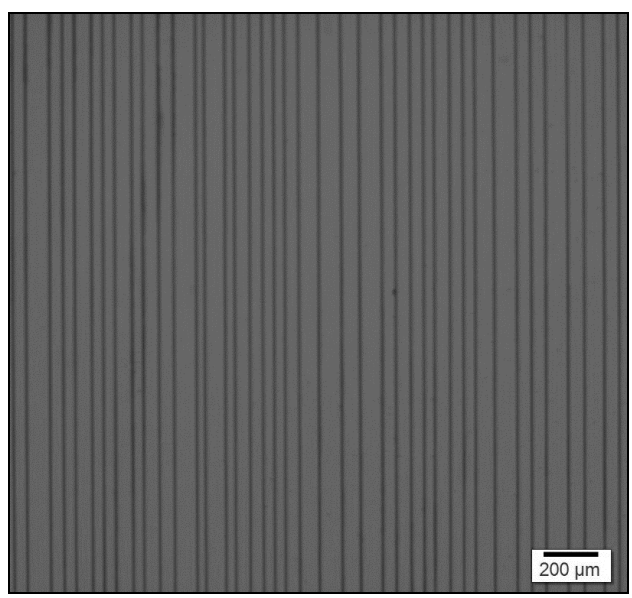

Figure 16.6 An array of cracks created by laser indentation process on 800 nm thick Si_3N_4 film on 550 um Si (100) substrate.

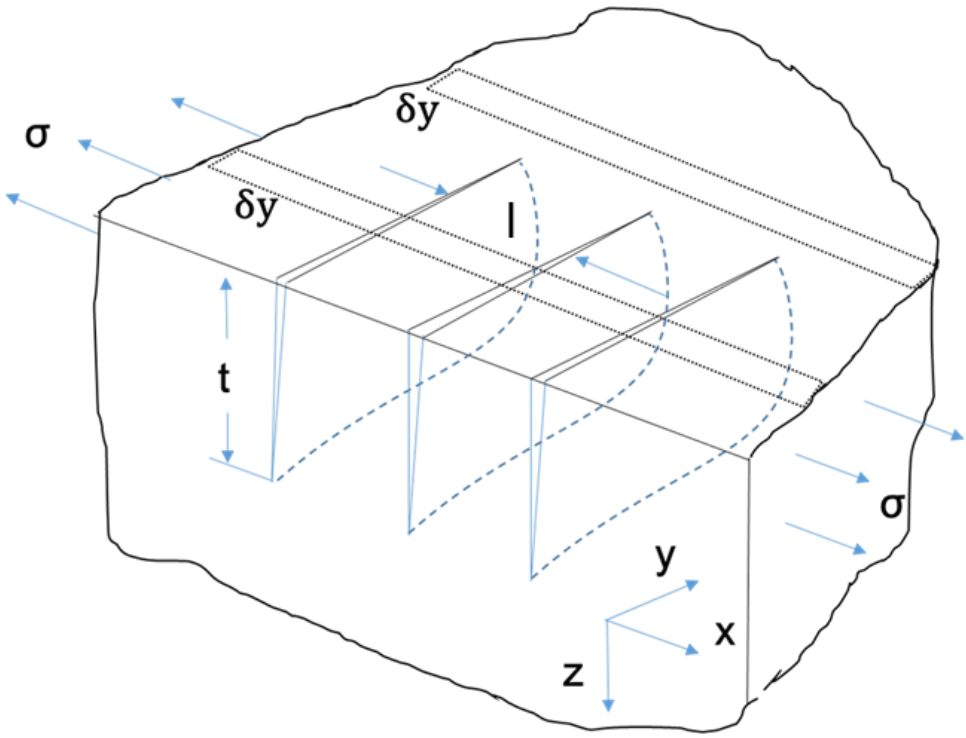

Figure 16.7 Schematic of parallel cracks with average spacing of l.

To determine pattern resolution or density of this technique, an experiment and a theoretical calculation on the minimum distance between cracks are conducted. Experimentally determined minimum distance between independent cracks is approximately 20 um for 800 nm Si_3N_4 film on 550um Si (100) as shown in Figure 16.6. To verify the experimentally attained value, theoretical calculation is conducted. Assuming the cracking medium is homogeneous and cracks propagate as depicted in Figure 16.7, average energy release rate of parallel cracks in y direction can be expressed as following,

$$G_y = \frac{\sigma}{t} \lim_{\delta y \to dy} \frac{\Delta U}{\delta y} \quad (4)$$

where t, σ, ΔU, δy are depth of penetration, remotely applied stress, change in elastic energy, and small strip of system. Also, the average energy release rate of parallel cracks in z direction, G_z, can be expressed in terms of dimensionless quantity, F(s) which only depends on depth of crack and spacing between the cracks[34]. G_z is defined as,

$$G_z = \frac{\sigma^2 \pi z (1-\nu^2)}{E} F(s)^2 \quad (5)$$

where E and ν are elastic modulus and Poisson's ratio. Since ΔU satisfies following,

$$\Delta U = \frac{\delta y}{l} \int_0^t G_z dz \quad (6)$$

Equating (4) and (5) using ΔU results following,

$$G_y \approx 1.98\sigma^2(1-\nu^2)t/E \qquad l \geq 8t \quad (7)$$

$$G_y \approx \left[\frac{0.5l}{t} - 0.0316\left(\frac{l}{t}\right)^2\right]\sigma^2(1-\nu^2)t/E \qquad l \leq 8t \quad (8)$$

where l is minimum spacing between two independent cracks as shown in Figure 16.7. Rewritten equation (8) in terms of critical stress intensity factor is, $K_{IC} = \sigma^{*}(t)^{1/2}$ when $l > 8$. Assuming substrate penetration is approximately 3 um, the stress is 300 Mpa and K_{IC} is 0.76 Mpa/$m^{1/2}$, the minimum distance is greater than 20 um since l is greater than 8t. Although the exact value of stress is not measurable due to technical difficulty, experimental value and calculated value show similarity.

Chapter 3.

Applications using crack manipulation

3.1 Nano/micro channel fabrication

There are various potential applications of the nanopatterns fabricated by manipulation of the oscillatory cracks. A fast and feasible application is to use the cracks as a nano/microchannel since the crack itself is naturally a channel structure. In addition, the cracks can easily be transferred to polydimethylsiloxane (PDMS) at wafer scale as shown in Figure 17a and 17b. The magnified optical image of a specific area, shown in Figure 17b, reveals transferred crack pattern into PDMS. As shown in Figure 17c, a three dimensional profile obtained via atomic force microscopy confirms that the embossed feature is the inverse of crack pattern, thus nanosize crack patterns can be easily transferred.

The nanosize channels are used in various fields, however pressure flow is almost impossible to generate in such size regime. To provide better utility for diverse channel applications, larger channel width is required. This can be achieved by wet etching of initial nanochannels made by crack manipulation. Figure 17d shows a multi-dimension channel fabricated by wet etching of existing cracks. Generally, adhesion between masking layer and substrate is important for microfluidic channel fabrication by wet

etching, otherwise additional deposition process is required; typically, a metal layer on the silicon substrate patterned via lift-off process is used. The minimum pattern resolution of conventional process using lift off process is up to 2 μm, thus creating features less than the minimium resolution is difficult especially by isotropic wet ethcing. However, the Si_3N_4 film adhere to Si substrate solidly as a masking layer, less than 2 μm features can be made with conventional etchant for instance HNA solution as shown in Figure 17d.[35] The strong adhesion of Si_3N_4 film to Si substrate also facilitates repetitive wet etching without additional deposition or patterning. Figure 17e shows the result of multiple isotropic wet etching. The channel width can be expanded up to several hundreds of micrometers under 10 min of total etching time.

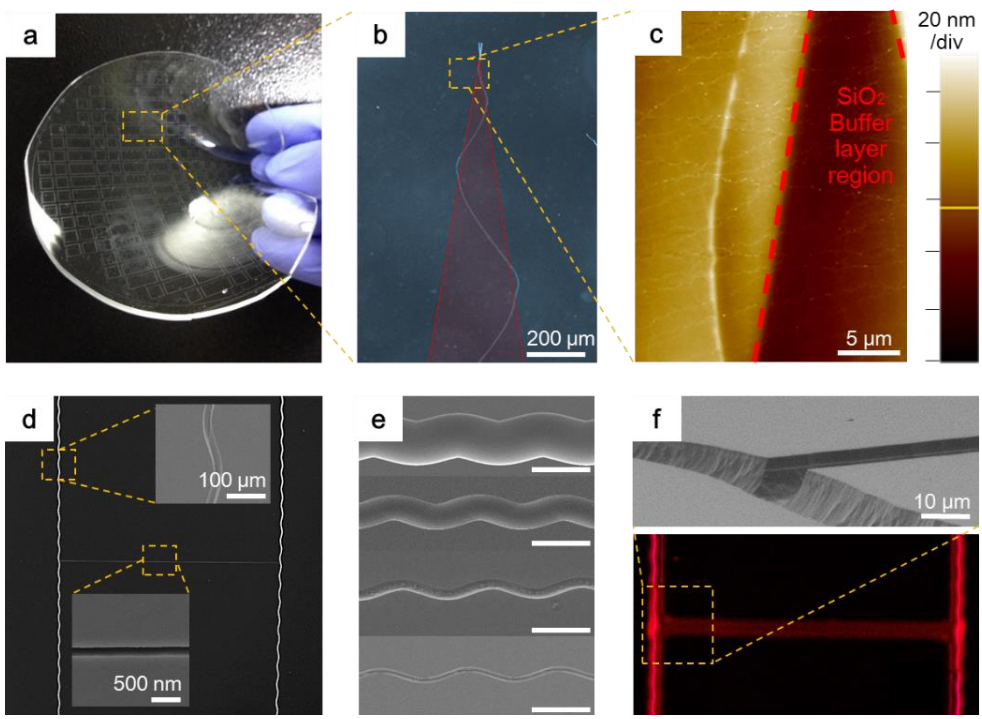

Figure 17. Application as nanochannel. (a) Crack patterns transferred at

wafer scale using polydimethylsiloxane (PDMS). (b) Optical microscopic image of inversed pattern of a nanocrack. (c) Atomic force microscope (AFM) image of transferred nanocrack. (d) Multi-scale channel fabricated by selective wet etching of existing cracks on (110) Si substrate. (e) SEM images of etched oscillatory cracks having various width. Scale bar: 100 μm (f) Intersection of widened channel by wet etching (top). Emission from quantum dot dispersed solution confined in the widened channel (bottom).

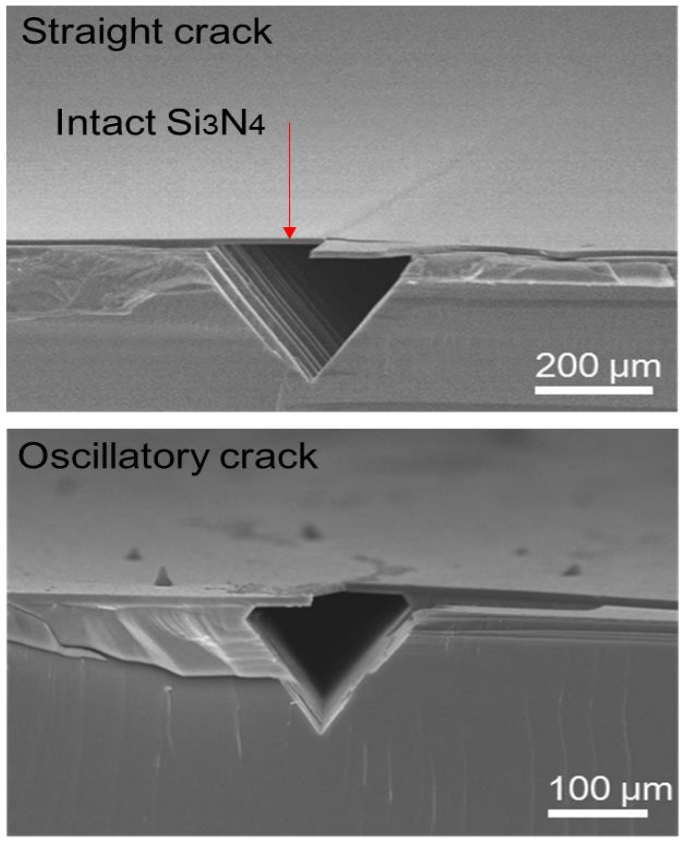

Figure 18. Microchannel fabrication via KOH wet etching. Top scanning electron microscope image shows a straight crack etched in KOH solution, and the bottom shows oscillatory crack etched in the same solution. Notice

the Si_3N_4 film is intact.

The channels fabricated by wet etching of the cracks are directly applicable to nano/micro fluidics. As shown in Figure 17f (top image), smooth top surface of the substrate is advantageous for PDMS or glass to adhere well for closed channel fabrication. As a demonstration of channel application, an expanded channel by isotropic wet etching capped with a PDMS block is filled with quantum dot dispersed solution as shown in Figure 17f (bottom image). Unlike isotropic wet etching, use of anisotropic etchant makes a triangular channel section profile as shown in Figure 18. In addition, the chemical reaction of anisotropic etchant including potassium hydroxide (KOH) or tetramethylammonium hydroxide (TMAH) is less volatile than using isotropic etchant, in turn the Si_3N_4 film adjacent to crack opening does not collapse or fracture after or during the etching process. This is advantageous since the Si_3N_4 film is still intact after etching is done as shown in Figure 18, thus the channel can be capped simply by bonding or spin coating of capping material.

In general, fabrication of nano/micro channels equivalent to those demonstrated in this study in width and length involves multiple lithography process or serial processes of electron beam lithography which is costly and time consuming. Using manipulation of the cracks obviate such difficulties, therefore the cost can be reduced greatly. It is expected that this study provides benefits in terms of utility and cost to many of those who do not

have an access to the state of art nanofabrication equipment in hand.

3.2 Transparent conductor fabrication using crack manipulation

3.2.1 Necessity of flexible transparent conductor

The necessity of flexible and robust transparent conductor is ever-growing due to rapid increase in the demands for next-generation large-area optoelectronic devices such as touch-screen display for human machine interface. Although the most viable alternative to indium tin oxide (ITO)[36] in terms of optical transparency and electrical conductivity is a metal mesh on plastic substrate including metal micro-lines at regular spacing and metal nanowire (NW) percolation network[37], its application to specific devices has been hampered by either moiré pattern[38] caused by the regular pattern or low mechanical robustness of the NW network. In this study, to overcome these shortcomings, a novel class of flexible transparent conductor based on metal NW micro-bundle network at random patterns is demonstrated in this study.

The original random patterns are prepared from high stress silicon nitride (Si_3N_4) on the silicon substrate (Si (100)), and utilized as repetitively usable mold with independently controllable pattern density and linewidth. Silver NWs are subsequently injected into the cracks through facile solution process and peeled off with the UV curable epoxy resin. The resultant

flexible and transparent conductor, spanning over wafer-scale at high reproducibility, not only exhibit enhanced mechanical robustness upon repeated bending or scratching, but also is free from moiré pattern due to the random nature of the NW bundle patterns. Further application of the resultant flexible transparent conductor as touch-screen panel confirms the superiority of the proposed scheme for easy fabrication of robust and flexible transparent conductor at large scale.

3.2.2 Current transparent conductors

Recently, interest in electrically conductive and optically transparent materials has increased in optoelectronics including solar cells [39] and touch-screen displays [40] as well as in thermo-electronical devices [41,42]. Indium Tin Oxide (ITO) and Fluorine Tin Oxides (FTO) have been abundantly used in the aforementioned field, however scarcity of the material and difficulties in the film deposition process [43-45] led to development of alternatives such as metal networks [46,47]. As compared to doped metal oxide films, ductility of the metallic networks is advantageous in terms of mechanical stability against deformations such as bending and stretching [48,49].

Amongst various metal networks, nanowire percolation networks have been studied widely as a substitute of the doped metal oxide film because of its high electrical conductivity, environmentally friendly deposition process, which does not necessitate high temperature or vacuum environment, and compatibility with solution process which enables large area or roll-to-roll process[50]. Nevertheless, there are still problems with industry level use of the nanowires such as imperfect uniformity of the nanowire networks when dispersed on a substrate and weak adhesion between the nanowires themselves or the nanowires and the substrate. Recently, as an alternative to the metal nanowire percolation networks, fracture assisted metallic network fabrication processes have been reported

[51-53] where random networks made by fracture of dried colloidal layers deposited on a flexible substrate is used as a template for subsequent metal deposition by sputtering or evaporation. The metal networks fabricated in this way however requires a metal deposition process via vacuum environment such as sputtering or evaporation process which increases the overall fabrication cost. In addition, the fracture pattern in the process varies each time thus electrical and optical properties of the resultant network may exhibit poor reproducibility. Nevertheless, both the metal nanowire percolation networks and the fracture assisted metal networks show high optical transmission and electrical conductivity simultaneously yet no optical moiré patterns observed due to randomness of the metal patterns.

3.2.3 Objectives for transparent conductor fabrication using cracking of thin film

In an attempt to develop a new approach that reduces the fabrication cost and still take an advantage of randomness of the metal network patterns which minimize the moiré effect, random fracture of glassy film deposited on a silicon substrate is utilized. As reported on several studies[17,22,28], high stress silicon nitride (Si_3N_4) on the silicon (Si) substrate leads to nanoscale random fractures in the film as well as the substrate by penetration of through thickness cracking. Using this randomly cracked glassy film/substrate as a template, metal nanowire networks on a transparent and flexible substrate can be fabricated. This new approach enables fabrication of transparent conductors composed of metal nanowire networks with a few micron scale line width. In addition, the film/substrate template can be used semi-permanently thus suitable for mass production. Via fracture pattern control and post process of the fractured substrate, fabrication of metal nanowire network patterns with various linewidths and pattern densities which are directly related to optical transmittance and electrical conductivity is demonstrated. In addition, by a simple resistive touch screen panel demonstration, the fabricated metal nanowire network patterns that can be directly applied to the device fabrication is verified in this study.

3.2.4 Transparent conductor fabrication using cracking of thin film

Figure 19 shows the overall process, schematically. A bare silicon wafer, either (100) or (110) is cleaned by standard wafer cleaning procedure. Without any additional patterning steps, silicon nitride (Si_3N_4) thin film is deposited through low pressure chemical vapor deposition (LPCVD) process. The deposition thickness is approximately 2 um to generate dense cracking of the Si_3N_4 film. The details regarding stress generation in this process will be discussed in the later chapter.

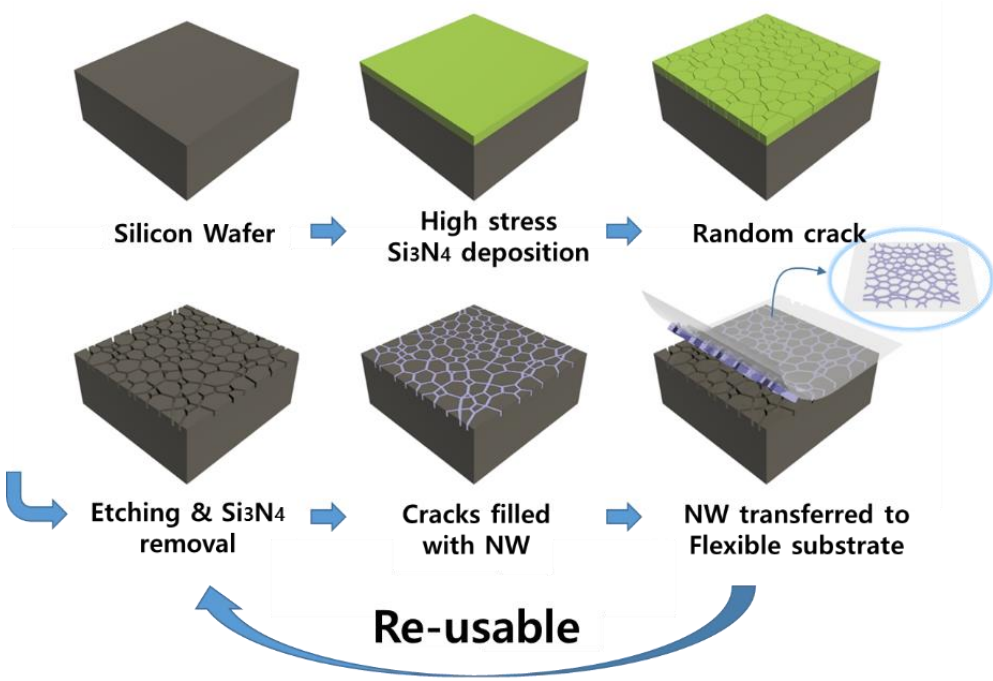

Figure 19 Schematic diagram of overall process: fabrication of transparent conductor using a template made by random crack of thin film.

Using the densely cracked Si_3N_4 film as a masking layer, Si substrate is etched selectively through wet etching process. Then Si_3N_4 is removed by selective etching solution. The crack patterns of the Si_3N_4 film is subsequently transferred to the Si substrate as shown in Figure 19. The patterns are filled with silver nanowires (AgNW) followed by light activated epoxy resin coated atop. The target substrate (PET film) is placed on the epoxy resin. The substrate peeled off after 30~40sec exposure under UV light. The AgNW is transferred onto the target substrate film as shown in the illustration. The Si substrate can be reused as a master template.

The high stress silicon nitride (Si_3N_4) film deposited on a silicon (Si) substrate induces substantial residual stress which exceeds fracture strength of the Si_3N_4 film. Since the fracture energy ratio between the Si_3N_4 film and the Si substrate Γ_s/Γ_f is small, substrate penetration is accompanied [31] upon the formation of the cracks. Under identical deposition condition that has been reported previously [22], the cracks having nanoscale width (100-150nm) begin to occur as the Si_3N_4 film thickness passes the crack initiation regime, approx. 800 nm [54].

As the film thickness is increased up to 2 um, the residual stress in the film is significantly increased, in turn a dense network of the nanocracks is produced. Since the cracks naturally have channel-like shape and Nano size width, when submerged in etching solution that selectively attacks the Si substrate such as HNA solution using silicon nitride film as a mask layer, a template having various line width and depth (several hundred nanometer

to several micrometers) can be fabricated. The template is subsequently filled with silver nanowire ink through razor blading. Then the UV curable epoxy resin is applied to promote adhesion between the filled nanowires and the flexible substrate which eventually be used as transparent conductor. Since the adhesion between the nanowires and the cured epoxy resin is much greater than mere Van Der Waals force between the nanowires and the Si substrate, the peeled-off film after curing under UV exposure transfers the nanowires well onto the film. As shown in Figure 20a, peeled-off PET film is highly transparent and flexible while the silver nanowire networks are formed along the random crack patterns of the template and maintain good electrical conductivity. The SEM image of peeled PET film shown in figure 20b and 20c shows multiscale patterns which have a network of nanowires within the random networks of microscale patterns.

As verified by EDS mapped image in figure 20d, Ag peaks are indicated in cyan color, the sliver nanowires form junction networks within micro scale channels. The nanowire junctions within the micro-sized pattern reduces the use of total nanowire content, and possibly the transmittance is increased as compared to random dispersion of the nanowire percolation networks. In addition, since the bundle of metal nanowires forms a fishnet like structure, is anticipated that higher mechanical stability against bending thus more suitable for flexible devices than the conventional metal networks made by sputtering or evaporation is anticipated.

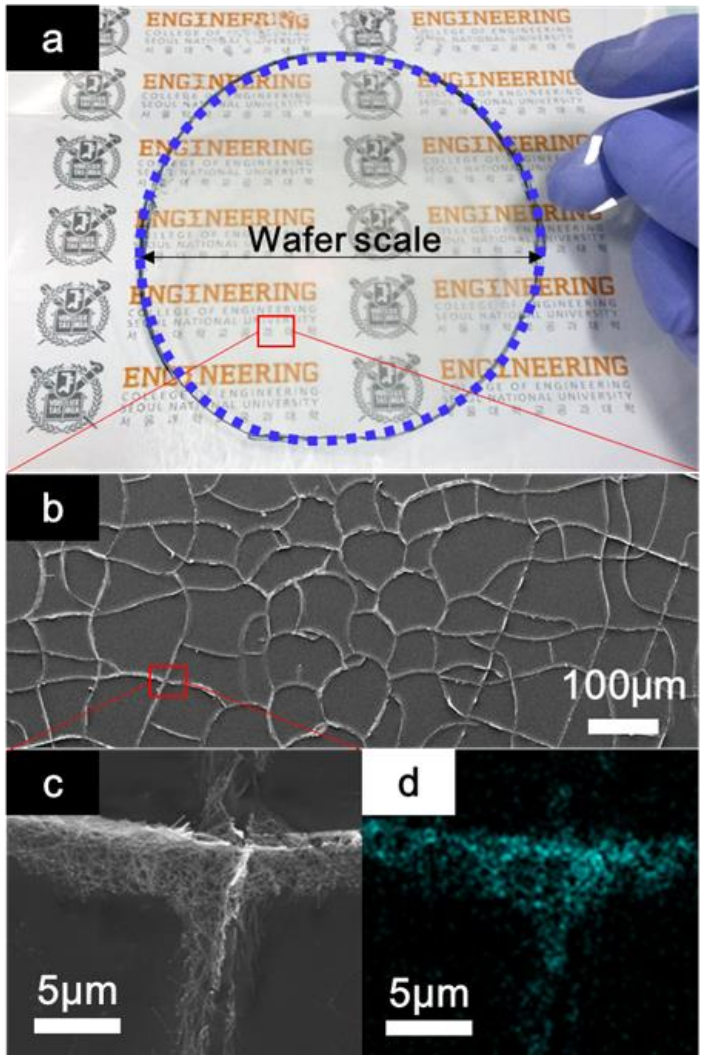

Figure 20. Fabrication of transparent conductor using a template made by random crack of thin film (a) Successfully peeled off flexible transparent conductor in wafer scale (b) Random network of metal lines consist of silver nanowires (c) Higher magnification SEM image at the junction of the random network (d) EDS mapping of Ag element (cyan color) in the corresponding SEM image confirming successful transfer of silver nanowire networks within microscale random patterns.

3.2.5 Master template fabrication and NW transfer to transparent film

Since the cracks are induced by the residual stress of the Si_3N_4 film which occur in wafer scale, as shown in figure 21a, a whole wafer can be patterned by random cracks without any lithographical process, thus no special patterning step is required. Initially, the cracks have nanoscale line width (100~150nm). This nanoscale width can be easily widened by HNA solution since etching selectivity of the Si3N4 over Si is extremely small [35,55]. Depending on the time and the concentration of the HNA solution, etched width and surface roughness varies [56]. As shown in figure 21b, various concentrations of the HNA solution has been tested for optimization of smooth channel profile.

The hardness of the silicon template enables repetitive use of the template. Figure 21c shows the template after 10^{th} use, yet no damages due to the blading process used for filling nanowires in the template is observed. Figure 21d, a cross section view of the template made by using the optimized HNA solution shows smooth section profile which is advantageous in peeling epoxy resin with nanowires. As shown in figure 21e peeled off epoxy resin has exactly the opposite cross section profile of the template. The nanowires initially filled in the template is successfully transferred onto the surface of the epoxy resin, as verified in a yellow color peak in EDS mapped image, shown in figure 21f.

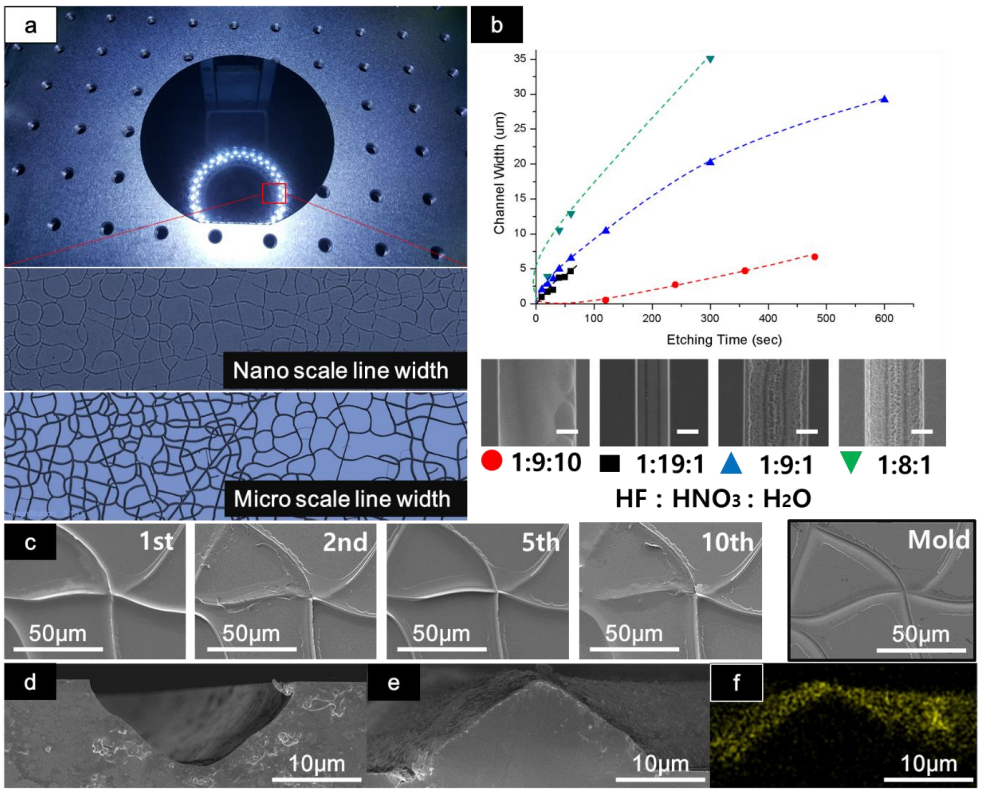

Figure 21. Lithography-free Patterned Si wafer and the properties of the channels widened by post wet etching. (a) Random cracks generated in wafer scale (top). Initial cracks with nanoscale line width (middle). Widened cracks after wet etching (bottom) (b) Etching rate of the cracks for different HNA mix ratio. Notice the surface profiles varies by HF content in the solution (c) SEM images of peeled off samples using a single template. (d) Section image showing a typical crack widened by optimized wet etching in the template. (e)-(f) Section image of a typical peeled off sliver nanowire networks and EDS mapped image showing silver nanowires on the surface in yellow peak

3.2.6 Control of pattern density using random cracking

The pattern density of the template can be controlled by regulating the Si_3N_4 film thickness. As shown in figure 22a, assuming that an enclosed are by random cracks is a grid size, the template made by thinner Si_3N_4 film corresponds to larger average grid size. As the Si_3N_4 film thickness is increased, the average grid size decreases and the variation in the grid size is reduced significantly. As shown in Gaussian distribution in figure 22b, the envelope of the distribution diminishes and a sharp peak appears as the Si_3N_4 film thickness is increased.

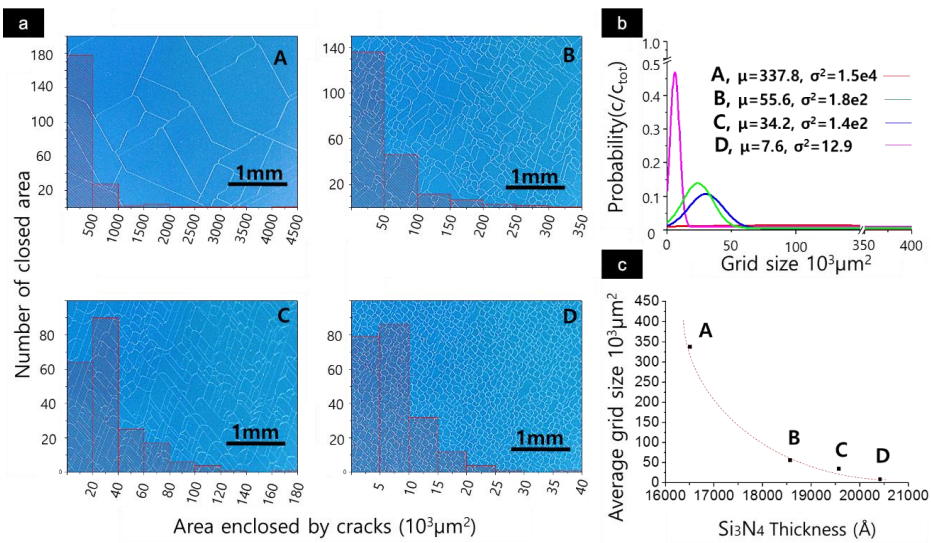

Figure 22. Density of cracks generated by residual stress of the Si_3N_4 thin film (a) optical microscope image of different density cracks. Notice that the crack density increases in alphabetical order, A to D (b) Gaussian distribution of grid size. (c) Graph of Si_3N_4 film thickness versus average grid size.

The mean values of each distribution correspond to the average grid size. For the Si_3N_4 film thickness 1.65 um, 1.85 um, 1.95 um, and 2.05 um, the corresponding average grid sizes are $7.6e^3um^2$, $34e^3um^2$, $56e^3um^2$, and $340e^3um^2$ respectively. As shown in figure 22c, the average grid size exponentially decreases as the Si_3N_4 film thickness increases, meaning that the silicon nitride (Si_3N_4) film thickness results in increased the residual tension. This result is in agreement with previously reported studies[54].

3.2.7 Optical, electrical, and mechanical properties of the transparent conductor

The optical transmittance of the random network of the silver nanowires transferred on a PET film is shown in figure 23a. The transmittance and the density of the crack or line width of the cracks have inversely proportional relationship. For simplicity, the line width silver nanowire networks is kept at 7um. Using typical PET film[57], the minimum relative transmittance of the networks made using the template with extremely high crack density (i.e. $8e^3um^2$ average grid size) is above 85% which is usable for optoelectronics device. Obviously, there is a tradeoff between optical transmittance and sheet resistance since the number of networks created by the random crack governs the sheet resistance. As shown in Figure 23b, the minimum sheet resistance is 120 Ω/□ for the high density sample. The sheet resistance exponentially increases as the grid size increases. In any cases of the density, no moiré is observed since all the networks are in random shape.

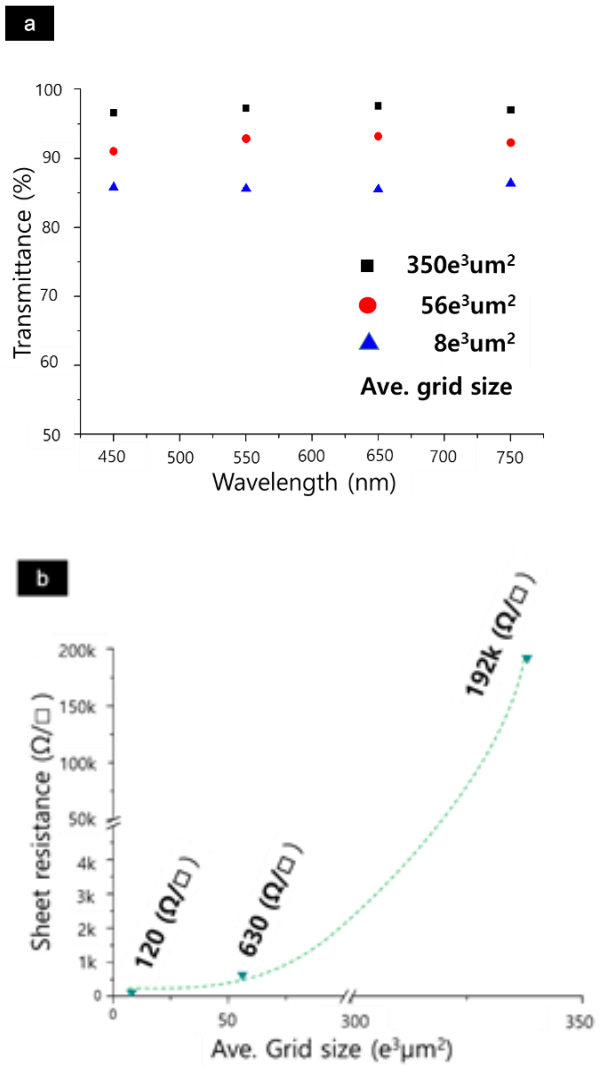

Figure 23. Optical and electrical properties of the silver nanowire networks transferred onto PET film. (a) Relative transmittance with PET reference for different average crack density of the template (b) Sheet resistance vs average grid size.

The silver nanowire networks made using the template show good mechanical stability against bending. This is mainly by good adhesion

between the nanowires and the PET substrate as well as by the property of nanowire network. As shown in figure 24a, over 2000 bending cycle, relative sheet resistance increase is less than 30% (R/R_0). Even after 6000 cycles, final sheet resistance increase is less than 10% (R/R_0) which proves that most of the jumps in the graph comes from the mechanical connection failure rather than failure of the electrode itself. Through a single peeling off procedure, a transparent conductor at a wafer size is readily prepared as shown in figure 24b. It substantiates that the size of the resultant transparent conductor is directly proportional to the size of the underlying wafer, showing potential scalability of this process. As shown in figure 24c, the transparent conductor fabricated in this manner can be directly used as touch screen panel. Different from a typical metal NW percolation network, the transparent conductor is not easily detached from the substrate or damaged by the mechanical abrasion that arises from operating the resistive type touch screen panel.

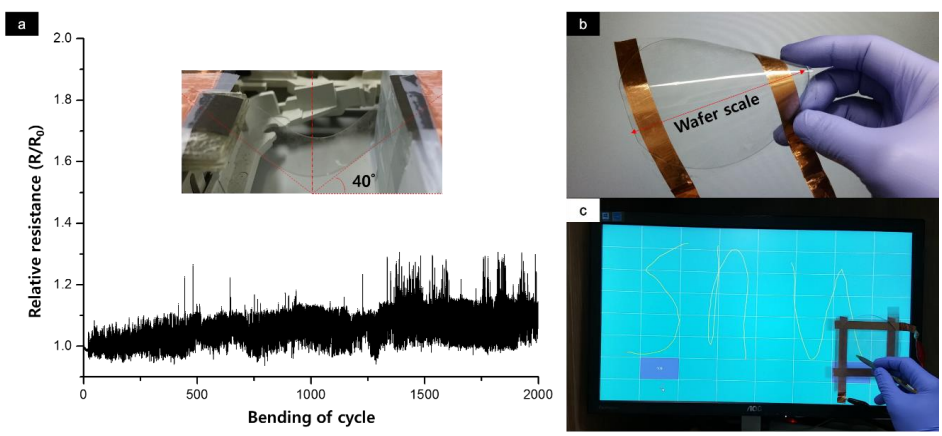

Figure 24. Mechanical properties of the transparent conductor fabricated

using random crack template. (a) Relative resistance versus bending cycle. Inset image shows 40˚ bending test. (b) Wafer scale touch screen panel fabricated using high density crack template. Notice no moiré appears in the panel (c) Touch screen test showing good sensitivity of the panel.

3.2.8 Transparent conductor fabrication using random crack filled with copper nanoparticles followed by laser sintering process

The silver nanowires have great electrical conductivity and mechanical stability by forming a fishnet like structure when the substrate is subjected to bending, however high material cost and weak adhesion to substrate than conventional ITO film or metal grids are disadvantageous for many applications which requires cost effectiveness. The demand for cost effective material has inclined recently as the transparent conductor market is ever-growing with the trend of flexible and transparent electronics. One of the most cost effective alternative material is copper nanoparticles (CuNPs). The material cost is much lower than the AgNWs, yet electrical conductivity of Cu (0.596×10^6 / cm·Ω) is comparable to that of Ag (0.63×10^6 / cm·Ω).

Two different methods are used to synthesize CuNPs. First, the CuNPs are synthesized by chemical reduction of copper ion in aqueous solution by dissolved copper acetate monohydrate in water is mixed with carboxyl acid and ammonia while stirring to increase the H^+ concentration required for copper reduction (pH = 10). Approximately in 1hr, the copper nanoparticles begins to form. Then, precipitated copper nanoparticles at the bottom when the stirring comes to stop are collected and cleaned with ethanol. Second method uses copper sulfate pentahydrate as a copper source. Polyvinylpyrrolidone (PVP, K-30) is mixed with sodium hypophosphite in

ethylene glycol with vigorous stirring. At 90˚C, is added in the solution. The copper nanoparticles begins to form at this stage and collected followed by acetone cleaning. Size of the CuNPs synthesized by this method is coarser than the other method, approximately 50 nm in diameter. As compared to first method, the grain size is much bigger, however the particle size is not a crucial factor especially when the pattern width of the mater mold is in micrometer scale which is several orders higher than 50 nm scale.

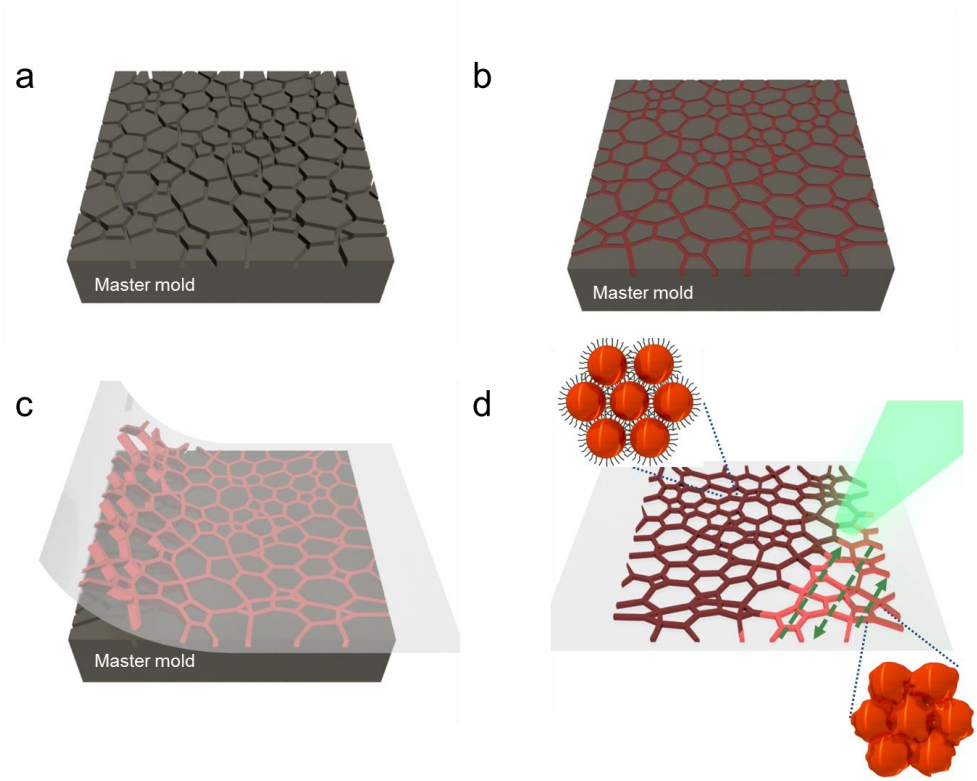

Figure 25. Fabrication process of copper based transparent conductor. (a) Si_3N_4 stripped random cracked Si substrate. (b) The Si substrate is filled with copper nanoparticles by razor blading process. (c) Epoxy resin coated

and ultraviolet exposure. (d) Visible laser (40 mW at 50 mm/s scanning speed) applied in large area for sintering Cu particles.

Overall copper based transparent conductor fabrication process is depicted in Figure 25. High concentration CuNP paste (> 10 wt%) is coated on the master mold prepared by random cracking of Si_3N_4/Si followed by Si selective wet etching. Using typical single blade razor, the master mold is filled with CuNPs and excess paste is removed. As shown in Figure 25b. The mold is then coated with epoxy resin followed by UV exposure and peeled off from the mater mold. Higher adhesion between the epoxy resin and the CuNPs enables complete transfer of CuNPs onto epoxy resin as shown in Figure 25d. At this stage, the CuNPs have high resistance due to oxidation from synthesis process. Thus additional process is required. Typical sintering process requires high temperature annealing, however such process is not applicable for this application unless the substrate material is thermally stable at high temperature. To overcome such problem, laser sintering process is conducted. The Nd:YAG laser, 40mW at 50 mm/s scanning speed, induces localized temperature field for reduction of copper oxide, yet the heat dissipation without much heat flux into the substrate. Thus, sintering of CuNPs is enabled with minimal damage to substrate.

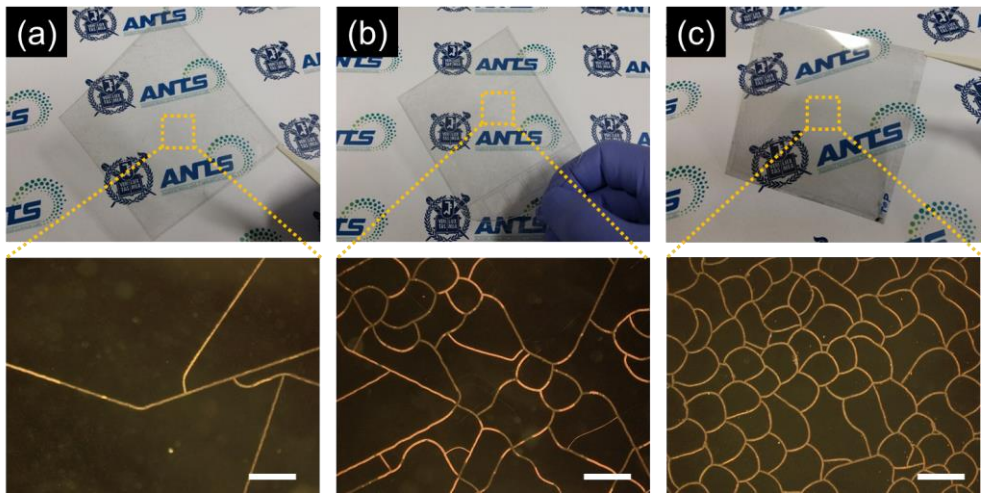

Figure 26. Fabricated copper based transparent conductor (top row). The crack density of master template which corresponds to copper pattern density in the fabricated transparent conductor increases in alphabetical order, (a) → (b) → (c). Scale bar: 200 um.

Figure 26 shows fabricated copper based transparent conductor. The density of conducting metal line made of sintered CuNPs can be controlled by pattern density of cracked master mold. As discussed in earlier chapter, the pattern density is closely related to the stored elastic energy of cracking medium: Si_3N_4/Si. There is a trade-off between density and optical/electrical conductivity which is discussed in later section of this study.

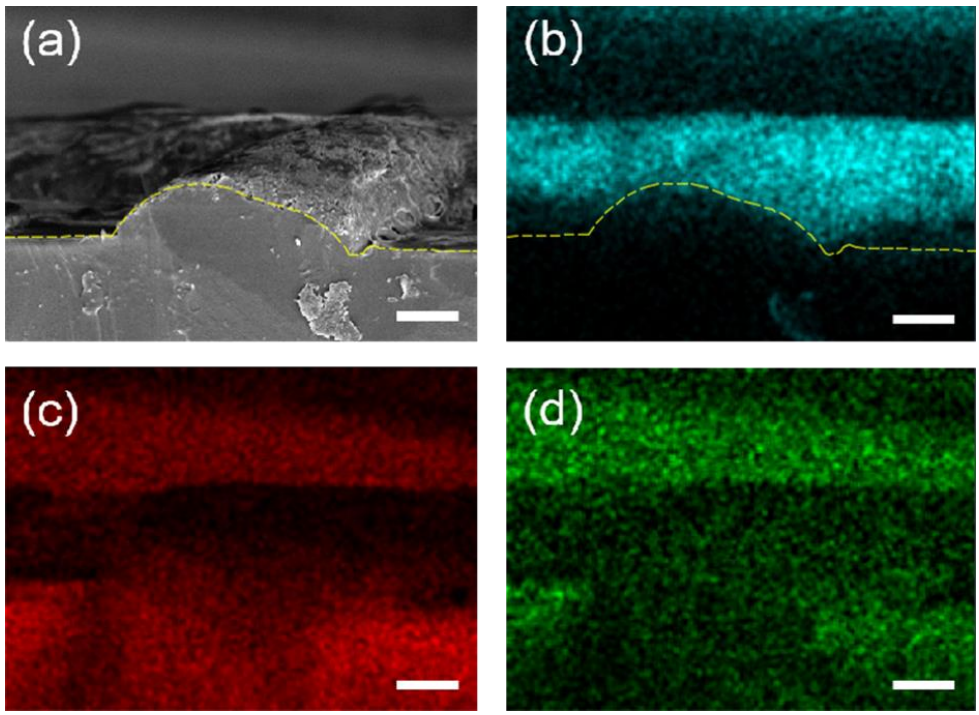

Figure 27. EDS image of copper based transparent conductor. (a) SEM image of cross section of a typical sample (b) Cu peak indicated in cyan color (c) - (d) C and H peaks indicating polymer based substrate.

Figure 27 shows a cross section image of copper based transparent conductor. Along the hemi-circular shape of embossed structure, CuNPs are transferred as shown in Figure 27a. This shape is the inverse of master template, showing that a thin layered structure of CuNPs are atop of epoxy resin. As compared to bulk conductor line, material usage is greatly reduced although resistance may increase.

3.2.9 Optical, electrical, and mechanical properties of the copper based transparent conductor

Optical property of the CuNPs based transparent conductor depends on the density of patterns and width. As the pattern width is decreased, the transmittance decreases as well. Study on the pattern thickness vs. transmittance is discussed in the earlier chapter. For simplicity, transmittance vs. pattern density is discussed. As shown in figure 28(a), average transmittance of visible wavelength regime is 84%, 90% and 95% depending on the density of the pattern. In case of lowest pattern density, the resistance of the transparent conductor is in MΩ/□ although the transparency is over 95%. In contrast, as shown in figure 28(b), the highest density transparent conductor has comparable sheet resistance with conventional ITO film as over 85% transmittance and under 20Ω/□.

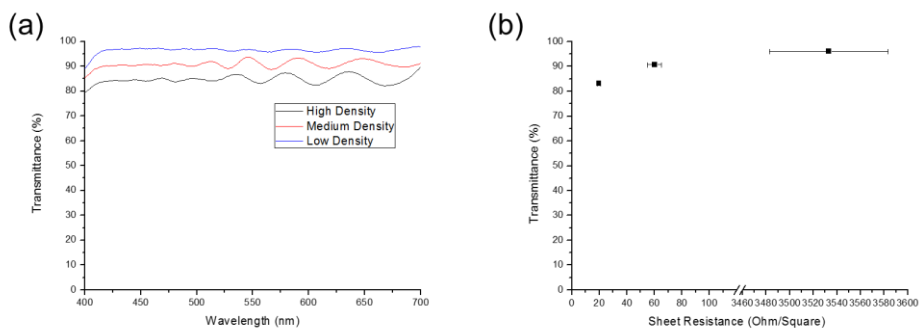

Figure 28. Fabrication process of copper based transparent conductor. (a) Si_3N_4 stripped random cracked Si substrate. (b) The Si substrate is filled with copper nanoparticles by razor blading process. (c) Epoxy resin coated

and ultraviolet exposure. (d) Large area laser applied for sintering Cu particle.

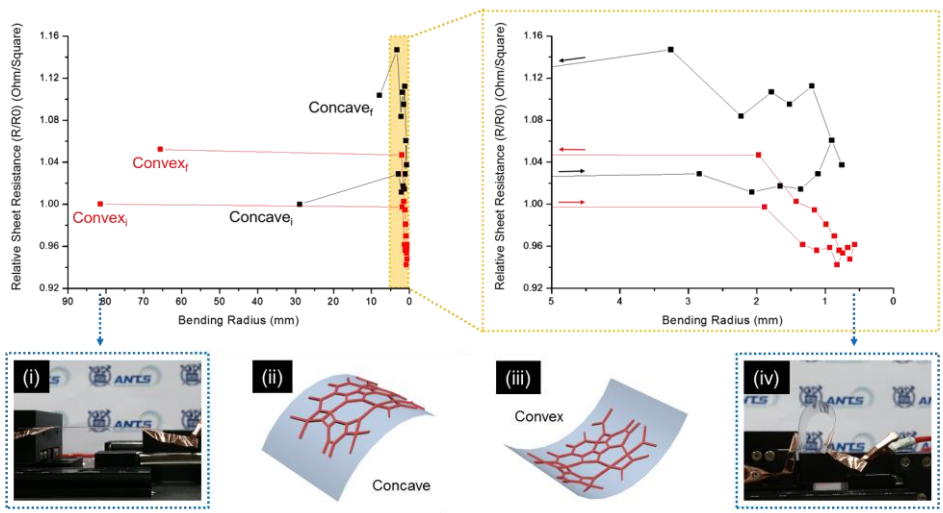

Figure 29. Sheet resistance of Cu based transparent conductor against bending in concave and convex direction.

The Cu based transparent conductor provide robust mechanical property against bending. As shown in figure 29, relative resistance is reduced at maximum bending radius of 0.5 mm. After cycle loading is finished in convex direction, less than 5 % of relative resistance increase is observed. For concave direction bending, maximum resistance increase is 15 %. After bending cycle is completed, total increase is 10 %. With conventional ITO film, these relative resistance increase is extremely hard to attain with equivalent bending condition.

In addition to robust mechanical property against bending, adhesion

of CuNPs to flexible substrate is notable. As shown in figure 30, the sheet resistance change after tape test is under 5 %. In contrast to typical AgNW based transparent conductor, this value is promising for resistive type touch screen panel since durability is assured.

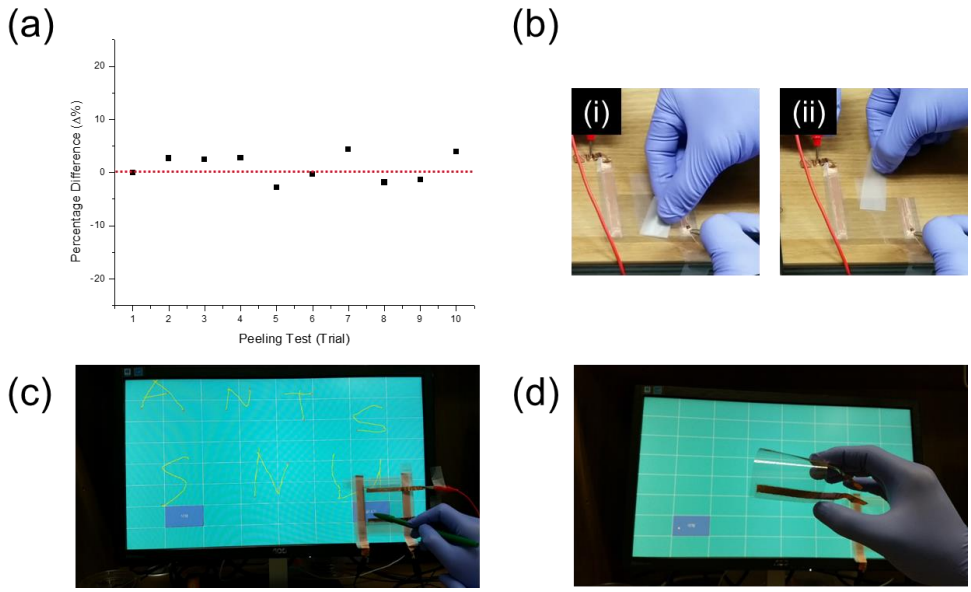

Figure 30. Robust adhesion to the substrate and application as touch screen panel are demonstrated. (a) Relative sheet resistance increase against peeling (b) Tape test using typical 3M tape is demonstrated. (c) Touch screen panel demonstration (d) flexible touch screen panel demonstration using Cu based transparent conductor.

Chapter 4.

Summary and future work

4.1 Summary

In this study, control and manipulation of different types of nanocracks and applications in large area nano/micro channel fabrication, transparent heater and conductor are demonstrated. The control of crack includes crack initiation and stop of oscillatory and straight cracks. The noble property of oscillatory crack arises from the substrate penetration of anisotropic surface energy of the substrate material which is (100) oriented silicon wafer. Utilizing this phenomenon, the wave-like properties of the oscillatory cracks are manipulated to demonstrate similarity of diffraction, amplification, total internal reflection, and evanescent wave of optical wave. In addition, the cracks made in this fashion can be expanded by post wet etching process, therefore utility for nano/micro pattern fabrication is proved.

In chapter 2 and 3, wet etched cracked substrate is employed as a template for large area nanopattern transfer to fabricate flexible and transparent conductors. Using AgNWs and CuNPs, highly durable and mechanically robust TSP is fabricated and demonstrated as resistive type

touchscreen panel. The optical properties are comparable to conventional ITO film which is most widely used in the latest electronics devices, thus viability as ITO alternative is proved.

4.2 Future work

In order to meet the increasing demand for flexible electronics in wearable device fabrication, development of cost effective transparent conductor fabrication technique is required. The transparent conductor fabrication technique demonstrated in this study utilizing random and controlled cracking of silicon based substrate can be expanded by employing various types of substrates including glass and polymer based substrates as long as sufficient stress is induced for cracking.

The Si wafer size is limiting factor in this study in terms of size of the final product. Expanding this technique on glass based substrates which can easily be made in larger dimension will increase the productivity and reduce the cost of the transparent conductor fabrication. Similar benefits are expected when polymer based substrate is used.

In addition, polymer substrates can provide a stretch-ability. For example, a stretchable substrate including PDMS can be easily patterned as shown in chapter 2 using the silicon template made by crack assisted patterning technique, expansion of application area into stretchable device fabrication is tangible task. Use of patterned substrate by crack assisted patterning provides good utility for highly transparent film without moiré effect is demonstrated in this study, thus stretchable and transparent without moiré pattern transparent conductor can be made as well.

Reference

1 Striemer, C. C., Gaborski, T. R., McGrath, J. L. & Fauchet, P. M. Charge-and size-based separation of macromolecules using ultrathin silicon membranes. *Nature* 445, 749-753 (2007).

2 Son, Y. *et al.* Nanoscale electronics: digital fabrication by direct femtosecond laser processing of metal nanoparticles. *Advanced Materials* 23, 3176-3181 (2011).

3 Tans, S. J., Verschueren, A. R. & Dekker, C. Room-temperature transistor based on a single carbon nanotube. *Nature* 393, 49-52 (1998).

4 Chen, Y. & Pepin, A. Nanofabrication: Conventional and nonconventional methods. *Electrophoresis* 22, 187-207 (2001).

5 Vieu, C. *et al.* Electron beam lithography: resolution limits and applications. *Applied Surface Science* 164, 111-117 (2000).

6 Ruess, F. J. *et al.* Toward atomic-scale device fabrication in silicon using scanning probe microscopy. *Nano Letters* 4, 1969-1973 (2004).

7 Binnig, G. & Rohrer, H. Scanning tunneling microscopy. *IBM Journal of research and development* 44, 279 (2000).

8 Binnig, G., Quate, C. F. & Gerber, C. Atomic force microscope. *Physical review letters* 56, 930 (1986).

9 Scheer, H.-C., Schulz, H., Hoffmann, T. & Torres, C. S. Problems of the nanoimprinting technique for nanometer scale pattern definition. *Journal of Vacuum Science & Technology B* 16, 3917-3921 (1998).

10 Kumar, A., Biebuyck, H. A. & Whitesides, G. M. Patterning self-assembled monolayers: applications in materials science. *Langmuir* 10, 1498-1511 (1994).

11 Bates, C. M., Maher, M. J., Janes, D. W., Ellison, C. J. & Willson, C. G. Block copolymer lithography. *Macromolecules* 47, 2-12 (2013).

12 Xia, Y. & Whitesides, G. M. Soft lithography. *Annual review of materials science* 28, 153-184 (1998).

13 Whitesides, G. M. & Grzybowski, B. Self-assembly at all scales. *Science* 295, 2418-2421 (2002).

14 Park, M., Harrison, C., Chaikin, P. M., Register, R. A. & Adamson, D. H. Block copolymer lithography: periodic arrays of~ 1011 holes in 1 square centimeter. *Science* 276, 1401-1404 (1997).

15 Chou, S. Y., Krauss, P. R. & Renstrom, P. J. Nanoimprint lithography. *Journal of Vacuum Science & Technology B* 14, 4129-4133 (1996).

16 Yuse, A. & Sano, M. Transition between crack patterns in quenched glass plates. *Nature* 362, 329-331 (1993).

17 Gorokhov, E., Prinz, V. Y., Noskov, A. & Gavrilova, T. A Novel

Nanolithographic Concept Using Crack-Assisted Patterning and Self-Alignment Technology. *Journal of the Electrochemical Society* 145, 2120-2131 (1998).

18 Chung, S., Lee, J. H., Moon, M. W., Han, J. & Kamm, R. D. Non-Lithographic Wrinkle Nanochannels for Protein Preconcentration. *Advanced Materials* 20, 3011-3016 (2008).

19 Kim, M., Ha, D. & Kim, T. Cracking-assisted photolithography for mixed-scale patterning and nanofluidic applications. *Nature communications* 6 (2015).

20 Deegan, R. D. *et al.* Wavy and rough cracks in silicon. *Physical Review E* 67, 066209 (2003).

21 Zhang, Z. *et al.* Wavy cleavage fracture of bulk metallic glass. *Applied physics letters* 89, 251917 (2006).

22 Nam, K. H., Park, I. H. & Ko, S. H. Patterning by controlled cracking. *Nature* 485, 221-224 (2012).

23 Kim, D., Makaram, P. & Thompson, C. V. Microscale oscillating crack propagation in silicon nitride thin films. *Applied Physics Letters* 97, 071902 (2010).

24 Irene, E. Residual stress in silicon nitride films. *Journal of Electronic Materials* 5, 287-298 (1976).

25 Hutchinson, J. W. Stresses and failure modes in thin films and multilayers. *Notes for a Dcamm Course. Technical University of Denmark, Lyngby*, 1-45 (1996).

26 Dundurs, J. Discussion:"Edge-bonded dissimilar orthogonal elastic wedges under normal and shear loading"(Bogy, DB, 1968, ASME J. Appl. Mech., 35, pp. 460–466). *Journal of applied mechanics* 36, 650-652 (1969).

27 Wortman, J. & Evans, R. Young's modulus, shear modulus, and Poisson's ratio in silicon and germanium. *Journal of applied physics* 36, 153-156 (1965).

28 Elliman, R., Spooner, M., Dall, T., Kim, T. & Fletcher, N. Oscillating cracks in glassy films on silicon substrates. *Philosophical Magazine* 87, 4893-4906 (2007).

29 Pérez, R. & Gumbsch, P. Directional anisotropy in the cleavage fracture of silicon. *Physical review letters* 84, 5347 (2000).

30 Danilewsky, A. *et al.* Crack propagation and fracture in silicon wafers under thermal stress. *Journal of applied crystallography* 46, 849-855 (2013).

31 Ye, T., Suo, Z. & Evans, A. Thin film cracking and the roles of substrate and interface. *International Journal of Solids and Structures* 29, 2639-2648 (1992).

32 Dundurs, J. Elastic interaction of dislocations with inhomogeneities. *Mathematical theory of dislocations*, 70-115 (1969).

33 Hutchinson, J. W. & Suo, Z. Mixed mode cracking in layered materials. *Advances in applied mechanics* 29, 191 (1992).

34 Tada, H., Paris, P. & Irwin, G. *The analysis of cracks handbook*. (New York: ASME Press, 2000).
35 Williams, K. R. & Muller, R. S. Etch rates for micromachining processing. *Microelectromechanical Systems, Journal of* 5, 256-269 (1996).
36 Minami, T. Present status of transparent conducting oxide thin-film development for Indium-Tin-Oxide (ITO) substitutes. *Thin Solid Films* 516, 5822-5828 (2008).
37 Lee, P. *et al.* Highly stretchable and highly conductive metal electrode by very long metal nanowire percolation network. *Advanced Materials* 24, 3326-3332 (2012).
38 Nishijima, Y. & Oster, G. Moiré Patterns: Their Application to Refractive Index and RefractiveIndex Gradient Measurements. *JOSA* 54, 1-4 (1964).
39 Granqvist, C. G. Transparent conductors as solar energy materials: A panoramic review. *Solar energy materials and solar cells* 91, 1529-1598 (2007).
40 Madaria, A. R., Kumar, A. & Zhou, C. Large scale, highly conductive and patterned transparent films of silver nanowires on arbitrary substrates and their application in touch screens. *Nanotechnology* 22, 245201 (2011).
41 Hong, S. *et al.* Highly Stretchable and Transparent Metal Nanowire Heater for Wearable Electronics Applications. *Advanced Materials* 27, 4744-4751 (2015).
42 Kang, J. *et al.* High-performance graphene-based transparent flexible heaters. *Nano letters* 11, 5154-5158 (2011).
43 Shigesato, Y., Koshi-Ishi, R., Kawashima, T. & Ohsako, J. Early stages of ITO deposition on glass or polymer substrates. *Vacuum* 59, 614-621 (2000).
44 Kawashima, T., Matsui, H. & Tanabe, N. New transparent conductive films: FTO coated ITO. *Thin Solid Films* 445, 241-244 (2003).
45 Na, S.-I., Kim, S.-S., Jo, J. & Kim, D.-Y. Efficient and flexible ITO-free organic solar cells using highly conductive polymer anodes. *Adv. Mater* 20, 4061-4067 (2008).
46 Wu, H. *et al.* Electrospun metal nanofiber webs as high-performance transparent electrode. *Nano letters* 10, 4242-4248 (2010).
47 Lee, J.-Y., Connor, S. T., Cui, Y. & Peumans, P. Solution-processed metal nanowire mesh transparent electrodes. *Nano letters* 8, 689-692 (2008).
48 Yeo, J. *et al.* Next generation non-vacuum, maskless, low temperature nanoparticle ink laser digital direct metal patterning for a large area flexible electronics. *PloS one* 7, e42315 (2012).
49 Lee, J. *et al.* Very long Ag nanowire synthesis and its application in a highly transparent, conductive and flexible metal electrode touch

panel. *Nanoscale* 4, 6408-6414 (2012).
50 Yerushalmi, R., Jacobson, Z. A., Ho, J. C., Fan, Z. & Javey, A. Large scale, highly ordered assembly of nanowire parallel arrays by differential roll printing. *Applied physics letters* 91, 203104 (2007).
51 Han, B. *et al.* Uniform self-forming metallic network as a high-performance transparent conductive electrode. *Advanced Materials* 26, 873-877 (2014).
52 Gupta, R. *et al.* Spray Coating of Crack Templates for the Fabrication of Transparent Conductors and Heaters on Flat and Curved Surfaces. *ACS applied materials & interfaces* 6, 13688-13696 (2014).
53 Rao, K., Gupta, R. & Kulkarni, G. U. Fabrication of Large Area, High-Performance, Transparent Conducting Electrodes Using a Spontaneously Formed Crackle Network as Template. *Advanced Materials Interfaces* 1 (2014).
54 Suh, Y. D. *et al.* Control and Manipulation of Nano Cracks Mimicking Optical Wave. *Scientific reports* 5 (2015).
55 Kovacs, G. T., Maluf, N. I. & Petersen, K. E. Bulk micromachining of silicon. *Proceedings of the IEEE* 86, 1536-1551 (1998).
56 Hamzah, A. *et al.* Optimization of HNA etching parameters to produce high aspect ratio solid silicon microneedles. *Journal of Micromechanics and Microengineering* 22, 095017 (2012).
57 Nakamura, T., Tsutsumi, N., Juni, N. & Fujii, H. Thin-film waveguiding mode light extraction in organic electroluminescent device using high refractive index substrate. *Journal of applied physics* 97, 054505 (2005).

Abstract

Manipulation of nanocracks on silicon based thin film and its application as large area nanopatterning

Suh Young Duk
Department of Mechanical and Aerospace Engineering
The Graduate School of Mechanical Engineering
Seoul National University

Generally, a fracture is considered as an uncontrollable phenomenon due to its highly random nature. The aim of this study is to investigate straight, random, and highly ordered cracks such as oscillatory cracks and to manipulate via elaborate control of mechanical properties of the cracking medium including thickness, geometry, and elastic mismatch. Utilizing semiconductor fabrication and laser technology, a specific thin film with micro-sized notches fabricated on a silicon based substrate generates various types of self-propagating nano-cracks in large area including optical wave-like nano-cracks resembling refraction, total internal reflection and evanescent wave. These novel properties are utilized to fabricate complex and large areal nano/micro patterns which is extremely difficult to fabricate using conventional nano/micro patterning process. The nano/micro patterns

made in this study are directly implementable into a nano/micro-channel application since the cracks naturally have a form of channel-like shape. In addition, a flexible transparent conductor fabrication using the nano/micro patterns as template is demonstrated.

Keywords : nanopatterning, fracture, crack, transparent conductor, crack assisted patterning